Topology Mediated Network Turing Patterns

University of Oxford

A dissertation submitted for the degree of

MSc in Mathematical Sciences

2024

Abstract

By extending a topological control mechanism originally proposed in [8], we seek to mediate Turing patterns on unweighted, undirected networks through topological tuning. We conduct numerical simulations to highlight properties of our mechanism while establishing theoretical expectations for the special case of the ring lattice. While our primary contribution is proving boundedness results involved in targeted destabilization, we also contribute to the growing body of literature regarding network Turing patterns across graph generation models.

We first contextualize network Turing patterns by rigorously developing the ideas of Turing instability, pattern-enabled systems, and Laplacian matrix properties. We thus use early chapters to carve a natural path towards the original results found in later chapters, starting with generalized reaction-diffusion systems and building to mean-field approximations. As we assume no prior knowledge, this work is suitable for the young mathematician interested in complex networks, pattern formation, and matrix theory. Importantly, this work stands against a backdrop of real-world applications, motivating the importance of this field in modeling natural phenomena.

Contents

Notation

G	A graph. Assumptions on edge and structural restraints are specified in context
e_{ij}	Edge between nodes i and j
$\mathcal{N}_i$	One-hop neighborhood of node i
A	Adjacency matrix of a graph
D	Diagonal degree matrix of a graph
L	Laplacian matrix, defined here as $A - D$ in accordance with existing literature on network Turing patterns (rather than the more common $D - A$)
J	Jacobian matrix
Λ_α	Laplacian eigenvalue, not to be confused with λ_α
$\phi^{(\alpha)}$	Laplacian eigenvector
λ_α	Dispersion relation eigenvalue, not to be confused with Λ_α
N	Number of nodes
k_i	Degree of node i
x	Position vector. Used for continuous media reaction-diffusion system
t	Time
Δ	Laplacian operator
Δ_{disc}	Discriminant of a polynomial, not to be confused with Δ
S	Reaction-diffusion system, parametrized by diffusion coefficients and reaction functions. Defined separately from the network on which the system operates
$\mathcal{S}_p$	Set of pattern-enabled systems

δ_{ij}	Kronecker's delta. Not to be confused with single-subscript delta variables (e.g. δ_τ)
$M^\dagger$	Conjugate transpose of matrix M. Note we avoid the use of M^* to indicate the conjugate transpose
$\mathrm{tr}(M)$	Trace of matrix M
$\det(M)$	Determinant of matrix M
$\mathrm{Re}(x)$	Real component of x
$\mathrm{Im}(x)$	Imaginary component of x
$\imath$	Imaginary number, $\imath = \sqrt{-1}$. Not to be confused with index i
$\langle \cdot \rangle$	Average value brackets. Used primarily in context of average degree
u, v	Species variables in the two species reaction-diffusion system
D_u, D_v	Diffusion constants, by convention $D_u, D_v > 0$
$f(\cdot), g(\cdot)$	Reaction functions

Chapter 1

Introduction

1.1 Background

1.1.1 Turing Patterns

In a 1952 paper [39], Alan Turing introduced a theoretical framework to explain the formation of complex patterns in biological systems. Inspired by the process of morphogenesis, this paper sought to describe the seemingly spontaneous emergence of patterns from uniform initial conditions. Though the most easily identifiable examples of these "Turing patterns" are found in the animal kingdom (e.g. zebra stripes, giraffe spots, fish skin), Turing's work has proven successful in describing phenomena across diverse domains, including but not limited to predator-prey dynamics [36, 37, 22], galactal formations [41], cell signaling pathways [16, 34], brain networks [29, 7], molecular crystallization [15], and epidemic modeling [38, 42, 13].

Notably, recent decades have expanded studies of Turing patterns beyond just continuous media, offering valuable insights into the dynamics of discrete structures and systems as well.

1.1.2 Reaction Diffusion Equations

The mathematical framework underpinning Turing's theory of pattern formation is the reaction-diffusion system. To illustrate, we'll consider a prototypical example of an activator-inhibitor system in continuous media.

$$\begin{cases} \dfrac{\partial u}{\partial t} = f(u,v) + D_u \Delta u \\ \dfrac{\partial v}{\partial t} = g(u,v) + D_v \Delta v \end{cases} \tag{1.1}$$

In the system described by (1.1), u is an activator whose growth is suppressed by v, an inhibitor. Both $u(\mathbf{x},t)$ and $v(\mathbf{x},t)$ are taken to represent the concentration

of a chemical species as a function of position and time. The functions $f(u, v)$ and $g(u, v)$ determine the reaction dynamics, while the Laplacian term accounts for their diffusion. Diffusion coefficients D_u and D_v are positive by convention. This formulation for the diffusive term is sound under the assumption of Fick's law, which states that the flux of a substance across a medium is proportional to its concentration gradient [23]. Turing patterns arise when the background medium develops stable activator-rich and activator-poor regions from uniform initial conditions.

| (a) Zebra stripes | (b) Reticulated giraffe | (c) Humphead Wrasse |

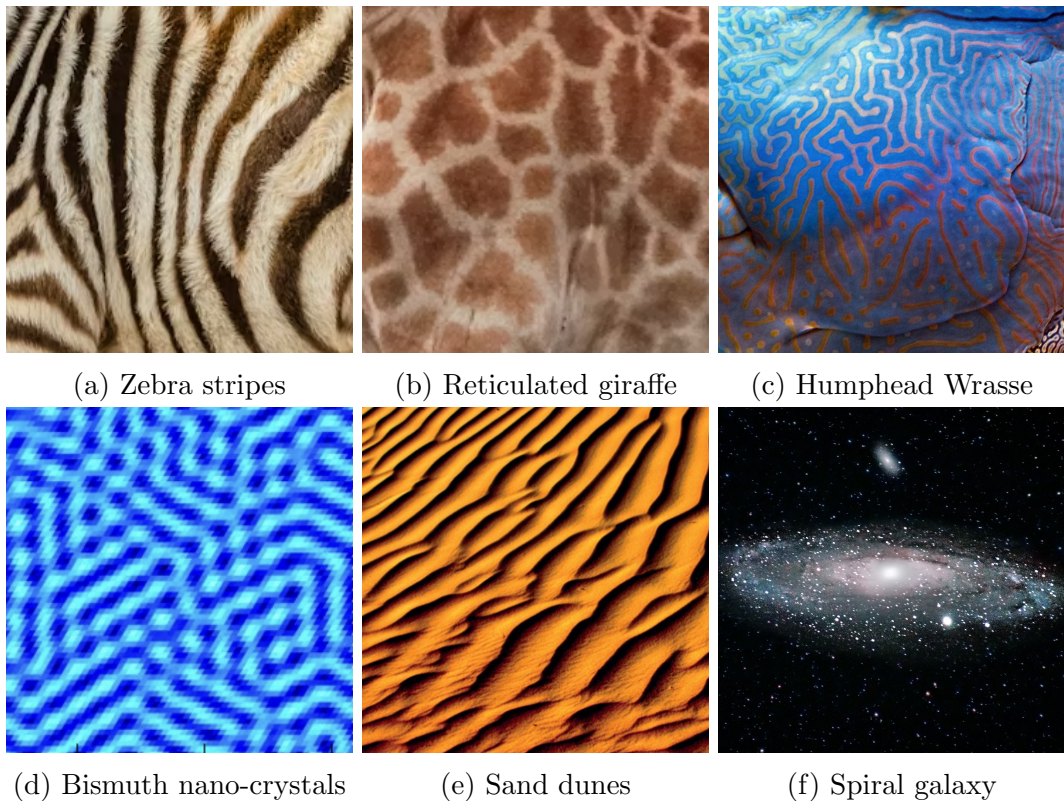| (d) Bismuth nano-crystals | (e) Sand dunes | (f) Spiral galaxy |

Figure 1.1: **Turing patterns in nature** [15]

Both the presence and nature of the formed patterns depend on the parameters of the system. For instance, by tuning the ratio of the diffusion coefficients, the system can be pushed from a state of stability, in which Turing patterns do not form, to a state of instability, where patterns spontaneously emerge, and vice versa.

The reaction-diffusion system contains the partial differential equations that describe concentrations of species as they interact and move about a continuous space; however, when using a network as the underlying substrate of interaction, we can adapt a discretized version of the reaction-diffusion system. We consider a system of differential equations for each node and use the network's Laplacian matrix to account for the diffusion of species.

$$\begin{cases} \dfrac{d}{dt}u_i = f(u_i, v_i) + D_u \sum_{j=1}^{N} L_{ij}u_j \\[3mm] \dfrac{d}{dt}v_i = g(u_i, v_i) + D_v \sum_{j=1}^{N} L_{ij}v_j \end{cases} \tag{1.2}$$

The discrete formulation is motivated by the fact that Turing patterns in real-world scenarios are often better understood through network structures. In ecological systems, where nodes represent habitat patches, we can study quantized populations of predators and prey interacting in a patchy environment [44]. In multicellular dynamics, where nodes represent cells, we can study neuronal signaling pathways [29], morphogenesis [20], or even cytokine networks [17]. In epidemiology, where nodes represent people, we can study how a disease propagates through a population [38]. Considering the prevalence of network structures, there is no dearth of examples where network Turing patterns merit study.

1.1.3   Structurally Mediated Patterns

As in the continuous case, the emergence of Turing patterns on networks can be controlled by manipulating the system parameters; however, this concept does not always map well to real-world scenarios. Consider the aforementioned example of disease propagation across a network of people. Under the susceptible-infected-susceptible (SIS) framework, though we can see the effect of altering infection/recovery/diffusion rates mathematically, it can be far more difficult to change the actual rates of infection/recovery/diffusion in practice. Rather than manipulating the system parameters, we can instead explore the topology of the underlying network, wherein structural changes may more readily correspond to real-world scenarios. In an epidemiology setting, this might translate to implementing quarantine measures or immunization campaigns to alter the disease-transmissible connections (edges) between people (nodes), while in ecological settings this might translate to climate-change induced flooding of land-bridges (edges) that connect two or more habitats (nodes). It is thus a worthy endeavor to analyze the interplay between network structure and pattern formation. As such, this work aims to provide a rigorous treatment of topologically mediated network Turing patterns to shed insight on real-world phenomena.

1.2 Overview of Discussion

The early chapters of this dissertation are dedicated to building and exploring the foundations for Turing patterns on networks. Chapter 2 provides a rigorous derivation of stability conditions, while Chapters 3 and 4 explore existing theoretical understandings of pattern-enabled systems and stabilization. This conversation naturally transitions to structural control mechanisms, during which we concretely identify the scope of original results presented in Chapter 5. We summarize and identify related open research questions in Chapter 6.

Chapter 2

Formal Derivation of Stability Conditions

We start with a general vectorized form of the network reaction-diffusion system.

$$\frac{d}{dt}\mathbf{w_i} = \underbrace{\mathcal{F}(\mathbf{w_i})}_{\text{reaction term}} + \overbrace{K \sum_{j=1}^{N} A_{ij}\mathcal{G}(\mathbf{w_j} - \mathbf{w_i})}^{\text{diffusion term}}$$

where $\mathbf{w_i} \in \mathbb{R}^m$, $\mathcal{F} : \mathbb{R}^m \to \mathbb{R}^m$, $\mathcal{G} : \mathbb{R}^m \to \mathbb{R}^m$, and $K \in \mathbb{R}$ is constant. The dynamics of m species of interest are locally specified at node i by $\mathcal{F}$ (the *reaction*), whereas $\mathcal{G}$ controls the dynamics of species moving between nodes i and j for $j \in \mathcal{N}_i$ (the *diffusion*).

2.1 Preliminary 1: Assumptions

Following inspiration from activator-inhibitor systems, we assume $m = 2$ and a linear, species-independent[1] design of $\mathcal{G}$, allowing us to decompose the general formulation into the commonly studied two-species system. Namely, when

$$\mathbf{w_i} = \begin{pmatrix} u_i \\ v_i \end{pmatrix}, \ \mathcal{F}(\mathbf{w_i}) = \begin{pmatrix} f(u_i, v_i) \\ g(u_i, v_i) \end{pmatrix}, \ \mathcal{G} = \begin{pmatrix} c_u(u_j - u_i) \\ c_v(v_j - v_i) \end{pmatrix} \implies$$

---

[1]This design is an intentional but not mandatory choice following from Fick's law. Additional mechanisms can be designed that account for a given species' diffusion as a function of the concentrations of all species rather than just that of the diffusing species. As an example, such a design might prove apt for predator-prey scenarios in which the movement of a prey species intuitively depends on both surrounding prey and predator populations.

$$\begin{cases} \dfrac{d}{dt}u_i = f(u_i, v_i) + D_u \displaystyle\sum_{j=1}^{N} L_{ij}u_j \\ \dfrac{d}{dt}v_i = g(u_i, v_i) + D_v \displaystyle\sum_{j=1}^{N} L_{ij}v_j \end{cases} \qquad (2.1)$$

where $D_u = Kc_u$ and $D_v = Kc_v$ represent diffusion coefficients. It is worth clarifying that we define the Laplacian as $L = A - D$, following the conventions of existing literature on network reaction-diffusion systems. For the remainder of this work, we assume connected graphs unless explicitly stated otherwise. In the absence of diffusion, we assume there exists a linearly stable stationary state $(u_i^\star, v_i^\star)$, implying the following conditions:

$$\begin{cases} \operatorname{tr}(J^\star) = f_u + g_v < 0 \\ \det(J^\star) = f_u g_v - f_v g_u > 0 \\ f(u_i^\star, v_i^\star) = g(u_i^\star, v_i^\star) = 0 \end{cases} \qquad (2.2)$$

where partial derivatives and $J^\star$, indicating the Jacobian of the system in (2.1), are evaluated at the stationary state. Unless otherwise indicated, this will be assumed for all partial derivatives for the remainder of this work. Here the stationary state is a homogeneous solution, as $\mathcal{G}$ annihilates in zero [9].

2.2 Preliminary 2: Dispersion Relation

Allowing diffusion to occur, we now consider the conditions under which the stationary state remains stable by linearizing a small perturbation about $(u_i^\star, v_i^\star)$.

For $(u_i, v_i) = (u_i^\star + \delta u_i, v_i^\star + \delta v_i)$, disregarding higher order terms from the first-order Taylor approximation yields

$$\begin{cases} \dfrac{d}{dt}(\delta u_i) = f_u \delta u_i + f_v \delta v_i + D_u \displaystyle\sum_{j=1}^{N} L_{ij}\delta u_j \\ \dfrac{d}{dt}(\delta v_i) = g_u \delta u_i + g_v \delta v_i + D_v \displaystyle\sum_{j=1}^{N} L_{ij}\delta v_j \end{cases} \qquad (2.3)$$

L is diagonalizable, so we can express δu_i and δv_i in terms of the orthonormal eigenvectors of L.

$$\delta u_i = \sum_{\alpha=1}^{N} c_\alpha(t)\phi_i^{(\alpha)} \quad \delta v_i = \sum_{\alpha=1}^{N} b_\alpha c_\alpha(t)\phi_i^{(\alpha)} \qquad (2.4)$$

Combining (2.3) and (2.4), we achieve the following:

$$\sum_{\alpha=1}^{N} c'_\alpha(t)\phi_i^{(\alpha)} = f_u \sum_{\alpha=1}^{N} c_\alpha(t)\phi_i^{(\alpha)} + f_v \sum_{\alpha=1}^{N} b_\alpha c_\alpha(t)\phi_i^{(\alpha)} + D_u(\sum_{\alpha=1}^{N} c_\alpha(t)\Lambda_\alpha \phi_i^{(\alpha)})$$

$$\sum_{\alpha=1}^{N} b_\alpha c'_\alpha(t)\phi_i^{(\alpha)} = g_u \sum_{\alpha=1}^{N} c_\alpha(t)\phi_i^{(\alpha)} + g_v \sum_{\alpha=1}^{N} b_\alpha c_\alpha(t)\phi_i^{(\alpha)} + D_v(\sum_{\alpha=1}^{N} b_\alpha c_\alpha(t)\Lambda_\alpha \phi_i^{(\alpha)})$$

Using the linear independence of eigenvectors, we get a system of equations[2] for each of N eigenmodes, indexed by α.

$$c'_\alpha(t) = f_u c_\alpha(t) + f_v b_\alpha c_\alpha(t) + D_u c_\alpha(t)\Lambda_\alpha$$

$$b_\alpha c'_\alpha(t) = g_u c_\alpha(t) + g_v b_\alpha c_\alpha(t) + D_v b_\alpha c_\alpha(t)\Lambda_\alpha$$

Limit-cycle solutions are possible for a periodic Jacobian [9], but we focus here on non-periodic solutions. For non-periodic solutions, $c_\alpha(t)$ takes the form of $c_\alpha(t) = Ce^{\lambda_\alpha t}$ where C is a constant. Simplifying and re-writing in matrix form, we obtain an important result: the *dispersion relation* that connects $\lambda_\alpha, \Lambda_\alpha$, and system parameters.

$$\lambda_\alpha \begin{pmatrix} 1 \\ b_\alpha \end{pmatrix} = \begin{pmatrix} f_u + D_u\Lambda_\alpha & f_v \\ g_u & g_v + D_v\Lambda_\alpha \end{pmatrix} \begin{pmatrix} 1 \\ b_\alpha \end{pmatrix} \tag{2.5}$$

We henceforth distinguish between λ_α and Λ_α as the dispersion and Laplacian eigenvalues respectively.

2.3 Preliminary 3: Stability Conditions

Closer analysis of the dispersion relation shows us its importance, as stability conditions are dictated by the sign of $\text{Re}(\lambda_\alpha)$. $\text{Re}(\lambda_\alpha) < 0$ implies stability, as perturbations will decay with time and return to the stationary state. If, for any α, $\text{Re}(\lambda_\alpha) > 0$, the perturbations will grow exponentially, leading to pattern formation. The point at which $\text{Re}(\lambda_\alpha) = 0$ is thus deemed the *instability threshold*, representing the transition point for pattern formation.

Proposition 2.3.1. *Given stability conditions in terms of the sign of $Re(\lambda_\alpha)$, we can write equivalent stability conditions in terms of the sign of the Jacobian's determinant evaluated at $(u^\star, v^\star)$.*

---

[2]More generally, we get N m-dimensional systems, for a total of Nm equations grouped by index.

Proof. The characteristic polynomial of (2.5) is quadratic in λ_α, yielding an exact solution: $\lambda_\alpha = (\frac{1}{2})(\mathrm{tr}(J_\alpha) \pm \sqrt{(\mathrm{tr}(J_\alpha))^2 - 4\det(J_\alpha)})$. Let Δ_{disc} denote the discriminant. For $\Delta_{disc} \leq 0$, $\mathrm{Re}(\lambda_\alpha) = \mathrm{tr}(J_\alpha)$, which is always negative given the assumptions in (2.2) and the real, non-positive eigenvalues of L, which we know via the Courant-Fischer-Weyl principle. We are thus only interested in discussing scenarios where $\Delta_{disc} > 0$ and we take the positive root of the discriminant, resulting in the following implications on the sign of the determinant.

$$\mathbf{Case\ 1} : \mathrm{Re}(\lambda_\alpha) = 0 \implies \det(J_\alpha) = 0$$
$$\mathbf{Case\ 2} : \mathrm{Re}(\lambda_\alpha) > 0 \implies \det(J_\alpha) < 0$$
$$\mathbf{Case\ 3} : \mathrm{Re}(\lambda_\alpha) < 0 \implies \det(J_\alpha) > 0$$

$\square$

When taking a closer look at the determinant, we note that its sign is specifically controlled by the term $\Lambda_\alpha(f_u D_v + g_v D_u)$. When sufficiently dominant, it will push the determinant into the negative (unstable) region.

$$\begin{cases} \mathrm{tr}(J_\alpha) = f_u + g_v + \Lambda_\alpha(D_u + D_v) < 0 \text{ (always true)} \\ \det(J_\alpha) = \Lambda_\alpha^2 D_u D_v + \Lambda_\alpha(f_u D_v + g_v D_u) + f_u g_v - f_v g_u \end{cases} \tag{2.6}$$

It is apparent that by strategically manipulating diffusion coefficients and/or the reaction functions f and g, we can induce instability; however, when holding such system parameters constant, the dispersion relation becomes a function of Laplacian eigenvalues. As the Laplacian spectrum serves as a proxy for the structure of the underlying network, we can thus strategically manipulate network structure to induce instability as well.

Chapter 3

Pattern-Enabled Systems

We introduce the descriptor *pattern-enabled* to describe systems whose parameters allow for the formation of patterns. Importantly, this does not guarantee the presence of Turing patterns, as we still depend on the Laplacian eigenvalues of the network. After establishing the necessary (but insufficient) parameter conditions for pattern formation, we discuss theoretical understandings of network Turing patterns through eigenvector localization and mean-field theory.

Given the assumptions introduced in (2.2), let S denote a reaction-diffusion system parametrized by diffusion coefficients (D_u, D_v) and reaction functions (f, g). Let $\mathcal{S}_p$ denote the set of systems for which pattern formation is possible.

Definition 3.0.1. *If $S \in \mathcal{S}_p$, S is a pattern-enabled system.*

3.1 Parameter Restrictions

3.1.1 Reaction Function

Proposition 3.1.1. *Given the assumptions in (2.2), $f_u < 0 < g_v$ or $g_v < 0 < f_u$ is a necessary condition for $S \in \mathcal{S}_p$.*

We begin by re-visiting the conditions of the stationary state Jacobian introduced in (2.6), stated here again for ease.

$$\begin{cases} \text{tr}(J_\alpha) = f_u + g_v + \Lambda_\alpha(D_u + D_v) < 0 \\ \det(J_\alpha) = \Lambda_\alpha^2 D_u D_v + \Lambda_\alpha(f_u D_v + g_v D_u) + f_u g_v - f_v g_u > 0 \end{cases}$$

When both $f_u, g_v > 0$, we violate our original assumption on the stability of the stationary state in the absence of diffusion. When both $f_u, g_v < 0$, the system is uninteresting, as the stability conditions are always fulfilled. We thus require $f_u < 0 < g_v$ or $g_v < 0 < f_u$ for instability.

3.1.2 Diffusion Ratio

Noting that $D_v = (f_v g_u - f_u g_v - \Lambda_\alpha g_v D_u)(\Lambda_\alpha^2 D_u + \Lambda_\alpha f_u)^{-1}$ when $\text{Re}(\lambda_\alpha) = 0$, we can generate bifurcation curves in (D_u, D_v) space to illustrate regions of stability.
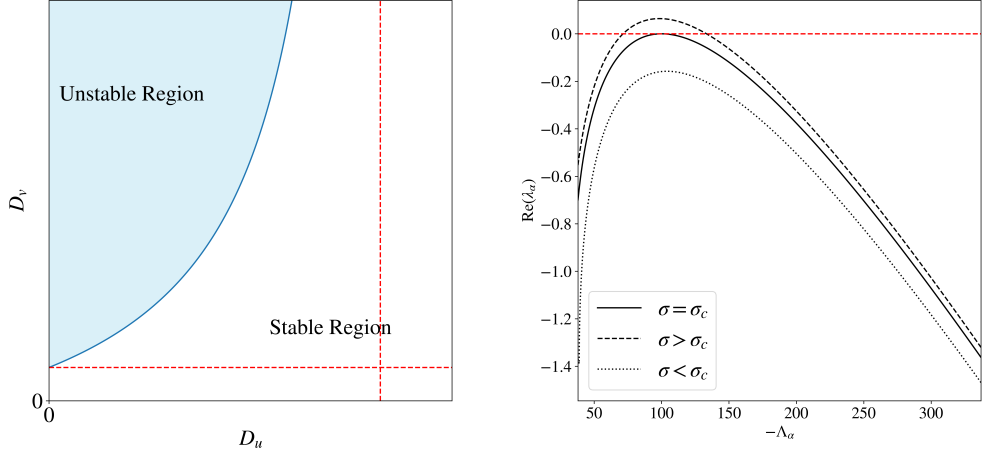
(a) **Bifurcation Curve:**
Sample stability regions for Λ_α

(b) **Dispersion Curve:**
Continuous dispersions for changing σ

Figure 3.1: System Parameter Curves

Each curve (see Figure 3.1a) splits the plane into stable and unstable regions for a given Laplacian eigenvalue, while points along the curve represent (D_u, D_v) pairs at a mode's instability threshold. Global stability is achieved for (D_u, D_v) pairs that lie below the bifurcation curve for all eigenvalues. Given both the vertical asymptote $(\frac{f_u}{-\Lambda_\alpha})$ and D_v-intercept $(\frac{f_v g_u - f_u g_v}{\Lambda_\alpha f_u})$ are inversely proportional to Λ_α, it is observed that the global stability region for large (D_u, D_v) is controlled by small Laplacian eigenvalues, while the opposite is true for small (D_u, D_v).

Proposition 3.1.2. *Given the assumptions in (2.2), $\sigma > \sigma_c$ is a necessary condition for $S \in \mathcal{S}_p$.*

Let σ denote the diffusion coefficient ratio, $\frac{D_v}{D_u}$. Manipulating D_u shifts the dispersion curve horizontally, while manipulating σ has the effect of vertically shifting the continuous dispersion curve as shown in Figure 3.1b and [30]. For the case in which the maximum value of the dispersion curve is 0, (i.e. $\text{Re}(\lambda)_{\max} = 0$), let σ_c denote the critical diffusion coefficient ratio. For $\sigma > \sigma_c$, an eigenmode can become unstable, while $\sigma < \sigma_c$ pushes the system back towards stability, as $\text{Re}(\lambda_\alpha)$ will always be less

than 0. Pattern-enabled systems thus require a choice of σ such that the dispersion curve crosses into the positive region, which, under our assumptions, means $\sigma > \sigma_c$.

3.2   Random Networks

We now couple our discussion of pattern-enabled systems with network structures. Random networks, suitable for modeling a diverse array of phenomena, are a natural starting point from which to build. Here we briefly review results for popular generation models.

3.2.1   Models

Erdős-Rényi (ER): An ER graph is parametrized by N and p, where $N \in \mathbb{Z}_+$ and $0 \leq p \leq 1$. N indicates the number of nodes, while an edge exists between each pair of nodes with independent probability p.

Watts-Strogatz (WS): A WS graph has an additional parameter κ, usually presumed to be an even integer. The graph is initialized as a ring lattice, wherein each node is connected to its nearest $\frac{\kappa}{2}$ neighbors on either side. In this model, each edge e_{ij} is independently re-wired with probability p to some new edge e_{il}, where node l is chosen uniformly at random while avoiding self-loops and edge duplication.

Barabási-Albert (BA): BA models produce scale-free networks with power-law degree distributions. A BA graph is characterized by two parameters, N and μ. As before, N denotes the number of nodes, while μ is typically presumed to be a positive integer smaller than N. The graph begins with an initial set of $\mu_0 \geq \mu$ connected nodes. At each step, a new node is added to the graph, along with μ edges that connect it to existing nodes. The probability of connecting the new node to an existing node i is proportional to the degree of node i, following the idea of preferential attachment. This results in a topology wherein a few nodes acquire a disproportionately high number of connections. Growth proceeds until the target number of nodes is reached.

3.2.2   Pattern-Enabled Parameter Space

As shown in [19], the parameter spaces in which Turing patterns form are quite different for random graphs from different generation models. For ER graphs, when manipulating N and p such that the average degree $\langle k \rangle$ remains the same, the stability-instability regions also remain nearly the same, suggesting a parameter

space highly dependent on $\langle k \rangle$. This makes some intuitive sense, as the degree to which the Laplacian spectrum can change is limited for constant $\langle k \rangle$, noting $N\langle k \rangle = \sum_{i=1}^{N} k_i = -\mathrm{tr}(L) = -\sum_{\alpha=1}^{N} \Lambda_\alpha$. For ER graphs in particular, Laplacian spectra are quite similar for graphs with equal $\langle k \rangle$, further supporting numerical results in [19]. Contrarily, WS graphs do not show the same consistency across average degrees, instead forming Turing pattern parameter spaces highly dependent on graph structure. Similar structural dependence is also found in scale-free networks, motivating further study as to how the Laplacian eigenvalues and eigenvectors depend on structure. Though not fully explored in [19], it is suggested that the differences are motivated by Laplacian eigenvector localization effects.

3.3 Localization

It is a well known phenomenon that eigenvectors tend to localize under certain conditions [18], often measured using an inverse participation ratio (IPR)[25].

$$\mathrm{IPR}(\phi) = \frac{\sum_i (\phi_i)^4}{(\sum_i (\phi_i)^2)^2} \tag{3.1}$$

Bounded between $\frac{1}{N}$ and 1, the IPR indicates the degree to which an eigenvector's "weight" is spread across its components; highly localized eigenvectors, where just a few components are responsible for the majority of the vector's weight, will have higher IPRs. It has been empirically shown that localization effects are generally more pronounced as degree heterogeneity increases; however, despite different levels of degree heterogeneity, ER, WS, and BA graphs alike all demonstrate strong degree-eigenvalue localization [18]. When nodes are sorted by decreasing degree and eigenvalues by decreasing absolute value, an eigenvector's characteristic localization degree (k_{α_c}) tends to correlate with its eigenvalue index—this is what is meant by degree-eigenvalue localization. An in-depth treatment of Laplacian eigenvector localization for large random networks is given in [18].

Conjecture 3.3.1. *For network Turing patterns on random graphs, local fields can be well-understood and approximated via a degree-dependent global mean-field.*

Notably, the strong degree-eigenvalue localization inspires the collective treatment of node dynamics with similar degrees. Adapting a similar approach to [31], Nakao and Mikhailov [30] provide empirical evidence for a mean-field approach to understanding pattern formation based on characteristic degrees of eigenvectors–an approach particularly well-suited to large networks with high degree heterogeneity.

The key insight to this approach is approximating a node's local-field by a global mean field. This approximation is shown for a species u below, where an identical process can be followed for species v.

$$\frac{d}{dt}u_i = f(u_i, v_i) + D_u(h_i^{(u)} - k_i u_i) \text{ where}$$

$$h_i^{(u)} = \sum_{i=1}^{N} A_{ij} u_j \approx k_i H^{(u)} \text{ and } H^{(u)} = \sum_{j=1}^{N} (\frac{k_j}{k_{total}}) u_j$$

Substituting in the approximation and combining with results for species v, we arrive at the global mean-field dynamics.

$$\begin{cases} \frac{d}{dt}u_i = f(u_i, v_i) + D_u k_i(H^{(u)} - u_i) \\ \frac{d}{dt}v_i = g(u_i, v_i) + D_v k_i(H^{(v)} - v_i) \end{cases} \tag{3.2}$$

Turing patterns have been shown in numerical simulations to be well-understood under this approximation, providing results consistent with the notion of a characteristic localization value controlled by the mobility of species (e.g. for u, $k_{\alpha_c} \propto -\Lambda_\alpha \propto \frac{1}{D_u}$). A full theoretical understanding is yet to be achieved as to why this is the case; however, a leading theory posits that networks with small diameters (e.g. small-world networks) facilitate fast diffusional mixing, which would allow us to explain pattern formation via a degree-based global mean-field approximation [30]. Ultimately, intuitions gleaned from the mean-field treatment of network Turing patterns leads us to question how localization effects might affect topological control mechanisms. With a robust understanding of instability conditions, pattern-enabled systems, and a preliminary theoretical framework to understand network Turing patterns, we are now ready to centralize the discussion in topology induced instability.

Chapter 4

Structural Tuning

We now supplement the discussion of necessary system conditions introduced in Chapter 3 with structural control mechanisms, defined here as strategic changes made to a network's topology to induce desirable Turing patterns. At the lowest level of abstraction, we focus on characteristics of Laplacian matrices, as we are essentially tuning the network until its Laplacian spectrum is desirable. At the highest level of abstraction, this is motivated by mapping real-world interventions to structural control strategies, leveraging mathematical insights to better understand formed patterns.

Most network typologies categorize networks by their structure and edge constraints, giving rise to temporal networks, multiplex graphs, hypergraphs, and trees among others, each of which typically has edges characterized as weighted/unweighted and directed/undirected. As topological tuning is still an emerging field, much of the early work has been dedicated to first understanding pattern formation on the aforementioned network types rather than structurally-mediating patterns [40, 4, 35, 3, 33]. Acknowledging the broad set of network types that similarly merit further study, we restrict our discussion here to undirected networks, with a particular emphasis on unweighted edges as well.

4.1 Laplacian Interventions

4.1.1 Stabilization via Re-weighting

Given a pattern-enabled system on an undirected graph with at least one unstable mode, how can we directly alter the Laplacian matrix to restore global stability?

Theorem 4.1.1. *Assume an undirected graph* $\mathbf{G}$ *and pattern-enabled system* $S \in \mathcal{S}_p$. *If at least one mode is unstable, there exists some Laplacian matrix* L^* *such that if* L *is replaced with* $L + L^*$, *global stability will be restored.*

This theorem follows from a "global topological control" mechanism adapted from [8], in which Cencetti et al. outline a procedure to manually push Laplacian eigenvalues into the stability region:

1. For each mode l, choose a δ_l such that $(\Lambda_l + \delta_l)$ yields a dispersion relation eigenvalue with negative real component.[1] If already stable, set $\delta_l = 0$.

2. Define a diagonal matrix D^* such that $D^*_{ll} = \delta_l$.

3. Calculate $L^* = \Phi D^* \Phi^T$ where Φ is a unitary matrix with orthonormal eigenvectors of L as its columns. [2]

4. Set $L_c = L + L^*$, henceforth deemed the *controlled Laplacian*

Lemma 4.1.1. *If L is Laplacian, L_c is also Laplacian.*

To substantiate this claim, we leverage strategies from [8] to show: 1) the elements of L_c are real and 2) column entries sum to zero. We begin by proving the entries of L_c are real.

Proof. Entries of L_c can be explicitly written in terms of eigenvalues, eigenvector entries and δ-shifts.

$$L_c = L + L^* = \Phi D \Phi^T + \Phi D^* \Phi^T = \Phi(D + D^*)\Phi^T \implies$$

$$(L_c)_{ij} = \sum_{k=1}^{n} \phi_i^{(k)} \phi_j^{(k)} (\Lambda_k + \delta_k)$$

For undirected $\mathbf{G}$, the eigenvalues, δ-shifts, and eigenvector entries are all real. Therefore $(L_c)_{ij} \in \mathbb{R}$. $\qquad\square$

In the above proof, we also implicitly show the eigendecomposition of L_c, with eigenvalues $\Lambda_\alpha + \delta_\alpha$ for $\alpha = 1, 2, \ldots, N$. Turning our attention to the column sums, we prove the final requirement for L_c to be Laplacian.

---

[1] Note that there is no sign guarantee on δ_l, as we can push the eigenvalue to either side of the unstable region of the dispersion relation. The original publication does not specify a convention.

[2] Since L is real symmetric Laplacian, we can choose an eigenbasis with all real eigenvector entries. We thus write Φ^T rather than the conjugate transpose $\Phi^\dagger$, knowing $\Phi^\dagger = \Phi^T = \Phi^{-1}$ in this case.

Proof. We expand the definition of the Laplacian eigenvalue in terms of the adjacency matrix

$$\Lambda_\alpha \phi_i^{(\alpha)} = \sum_j L_{ij} \phi_j^{(\alpha)}$$
$$= \sum_j (A_{ij} - \delta_{ij} k_j) \phi_j^{(\alpha)}$$
$$= \sum_j A_{ij} \phi_j^{(\alpha)} - k_i \phi_i^{(\alpha)}$$
$$= \sum_j A_{ij} \phi_j^{(\alpha)} - \sum_m A_{im} \phi_i^{(\alpha)}$$

Summing over i, we show $\sum_i \phi_i^{(\alpha)} = 0$, so long as $\phi^{(\alpha)}$ does not correspond to $\Lambda_\alpha = 0$.

$$\sum_i \Lambda_\alpha \phi_i^{(\alpha)} = \sum_{i,j} A_{ij} \phi_j^{(\alpha)} - \sum_{i,m} A_{im} \phi_i^{(\alpha)} = 0$$
$$\implies \sum_i \phi_i^{(\alpha)} = 0$$

When $\Lambda_\alpha = 0$, the summation becomes 0 directly. Using this information, the column sums of L^* therefore equal 0.

$$\sum_i L_{ij}^* = \sum_{i,k} \phi_i^{(k)} \phi_j^{(k)} \delta_k$$
$$= \sum_k \phi_j^{(k)} \delta_k \sum_i \phi_i^{(k)}$$
$$= 0$$

The column sums for both L and L^* are zero, since we already know L is Laplacian. We now arrive at the desired result for L_c.

$$\sum_i (L_c)_{ij} = \sum_i L_{ij} + \sum_i L_{ij}^* = 0$$

$\square$

We re-state without proof the complementary results that if L is balanced and symmetric, so is L_c, with full details provided in [8]. The eigenvalues of L_c are, by construction, all stable. In combination with Lemma 4.1.1, we have now shown Theorem 4.1.1 to be true.

As L_c is Laplacian, we can interpret it as representing an underlying graph. Though the shift from $L \to L_c$ is, superficially, a strategy to shift eigenvalues, we

can compare the underlying graphs generated by L and L_c to uncover the structural changes needed to mediate stabilization. Ultimately, we have created a Laplacian matrix whose eigenvalues are all stable by construction.

We now take a closer look at this transformation, paying particular attention to network structure. For the following observations, let $\mathbf{G}$ and $\mathbf{G}_c$ denote the graphs of interest recovered from L and L_c respectively. We additionally order δ-shifts such that $\delta_1, \delta_2, \ldots, \delta_N$ correspond to the ranked eigenvalues, $\Lambda_1 < \Lambda_2 < \ldots < \Lambda_N = 0$

Corollary 4.1.1. *For undirected* $\mathbf{G}$, *(i.e.* L, L_c *are both symmetric), the transformation* $L \to L_c$ *is equivalent to re-weighting each possible edge of* $\mathbf{G}$.

We can write the re-weighting exactly by taking a closer look at off-diagonal entries of L_c.

$$
\begin{aligned}
(L_c)_{ij} &= \sum_{k=1}^{n} (\phi^{(k)})_i (\phi^{(k)})_j (\Lambda_k + \delta_k) \\
&= \sum_{k=1}^{n} (\phi^{(k)})_i (\phi^{(k)})_j (\Lambda_k) + \sum_{k=1}^{n} (\phi^{(k)})_i (\phi^{(k)})_j (\delta_k) \\
&= L_{ij} + \underbrace{\sum_{k=1}^{n} (\phi^{(k)})_i (\phi^{(k)})_j (\delta_k)}_{:=\eta(i,j)}
\end{aligned}
$$

Here we see the transformation as an additive re-weighting by $\eta(i,j)$. With no further assumptions on $\mathbf{G}$, we make no further claims on the sign or bounds of $\eta(i,j)$. Thus, L_c represents a weighted, undirected graph that allows for negative weights.[3] As a final note, this re-weighting operates on edges and non-edges alike.

Corollary 4.1.2. $\eta(i,j)$ *is strongly influenced by eigenvectors with high IPR.*

If any $\phi^{(l)}$ is highly localized around some subset of nodes, then δ_l's contribution to $\eta(i,j)$ will be heavily weighted if i,j are included in the subset and hardly weighted otherwise. Accordingly, if all eigenvectors are highly localized, then $\eta(i,j)$ is essentially controlled by only the eigenvectors wherein i,j are in the localization subset.

---

[3]Though not universally appropriate for modeling real-world phenomena, negative-weights are salient in a number of network science applications, including financial and transportation networks among others.

Chapter 5

Targeted Destabilization

In chapter 4, we reviewed a topological control mechanism that, when implemented, prevents pattern formation on an undirected graph by re-weighting its edges, with no sign-restriction on weights. Can we instead develop a control mechanism where, rather than re-weighting, we add/delete/re-wire unweighted edges to induce instability on targeted modes?
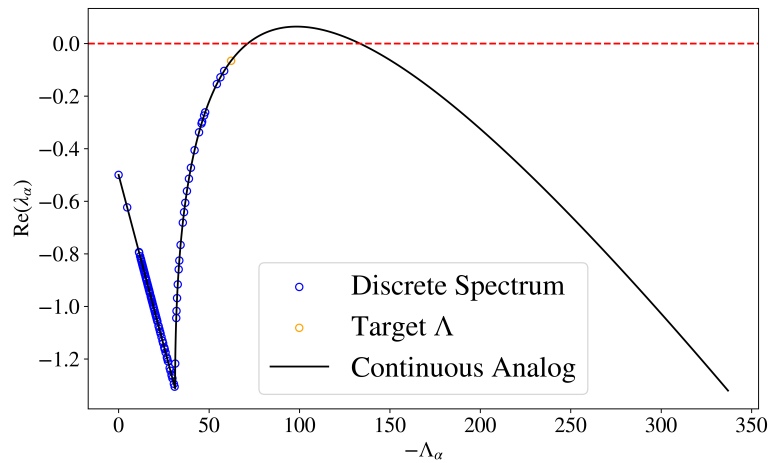

Figure 5.1: **Initial Setup** — Continuous and discrete dispersion relation

Suppose we have an undirected, unweighted graph $\mathbf{G}$ and $S \in \mathcal{S}_p$ whose continuous dispersion relation crosses the instability threshold at two points, Λ_{c_1} and Λ_{c_2}, with $\Lambda_{c_1} < \Lambda_{c_2}$. The Laplacian spectrum of $\mathbf{G}$ is ordered[1] $\Lambda_0 < \Lambda_1 < \ldots < \Lambda_{N-1} = 0$. Suppose further the Laplacian spectrum lies entirely in the stable region and pattern formation does not occur. In other words, $-\Lambda_\alpha < \Lambda_{c_1}$ or $-\Lambda_\alpha > \Lambda_{c_2}$ for all $\alpha = 0, 1, \ldots, N-1$.

---

[1]We change index from 0 to $N-1$ for ease of notation in future circulant matrix calculations.

If we imagine the continuous dispersion relation as a string, and the discrete eigenvalue dispersions as beads on that string, we seek to select just one bead and slide it along the string into the unstable region, while 1) recovering an undirected, unweighted graph from the altered Laplacian spectrum and 2) keeping the other beads (eigenvalues) as close to their original value as possible. This setup is shown in Figure 5.1.

5.1 Weight-Collapse

We use the control mechanism outlined in Chapter 4 as a starting point. When seeking to destabilize just one mode, we alter the first step of the procedure slightly.

1. (New) After identifying a target mode τ, choose a δ_τ such that $\Lambda_\tau + \delta_\tau$ lies in the instability region, while $\delta_l = 0$ otherwise.

Subsequent steps to generate L_c remain the same. With only one non-zero δ-shift, we achieve a simpler form for $\eta(i, j)$, which we now index by τ.

$$(L_c)_{ij} = L_{ij} + \eta^{(\tau)}(i, j)$$
$$\eta^{(\tau)}(i, j) = (\phi^{(\tau)})_i (\phi^{(\tau)})_j (\delta_\tau)$$

We desire a Laplacian L_f such that $(L_f)_{ij} = \{0, -1\}$ for $i \neq j$, and $(L_f)_{ii} = \sum_{j \neq i}(L_f)_{ij}$. To achieve this, we propose a simple step function, $\mathcal{W} : \mathbb{R} \to \mathbb{R}$, that collapses values of $\eta^{(\tau)}(i, j)$ depending on some threshold parameter $\theta \in (0, 1)$.

$$\mathcal{W}(x) = \begin{cases} -1 & \text{if } x \leq -\theta \\ 0 & \text{if } x > -\theta \end{cases}$$

After applying this function to off-diagonal entries of L_c, we re-define diagonal entries by calculating row sums of the altered matrix, adding steps (5) and (6) to the control mechanism procedure to form our new matrix L_f, whose eigenvalues are denoted $\Lambda_\alpha^{(f)}$.

5. Form off-diagonal entries of L_f, where $(L_f)_{ij} = \mathcal{W}((L_c)_{ij})$

6. Form diagonal entries of L_f, where $(L_f)_{ii} = \sum_{j \neq i}(L_f)_{ij}$

Steps (5) and (6) successfully form L_f such that its underlying graph is undirected and unweighted. The transformation $L \to L_f$ can thus be conceptualized as adding, deleting, or re-wiring edges of L if intermediate re-weightings (captured by L_c) cross a certain threshold θ. Though we have the desired form for L_f, given the intractable nature of analytically deriving the eigenvalues of L_f, there is no clear guarantee that we achieve the desired Laplacian spectrum. We thus turn towards numerical simulations to empirically evaluate the success of this weight-collapse approach.

5.2 Numerical Simulations

5.2.1 Set-up

Our simulation recipe involves four components: a graph, system parameters, procedural variables, and evaluation criteria.

Graph Choice: We are interested in connected graphs with unweighted, undirected edges. Initial simulations were conducted on ER, WS, and BA graphs, as well as ring lattices[2]. The ring lattice as a graph structure of choice was intentional, as we can exploit its structure to compare theoretical expectations against empirical results. We therefore give special attention to and conduct additional simulations on the ring lattice.

System Parameters: A number of popular models are used to define the local (reaction) dynamics of species, including but not limited to the Mimura-Murray, Ginzburg-Landau, FitzHugh–Nagumo, and Brusselator models [27, 47, 32, 1]. Without loss of generality, we use the Brusselator model defined below on parameters $\alpha = 2$ and $\beta = 4$:

$$f(u_i, v_i) = \alpha - (\beta + 1)u_i + u_i^2 v_i$$
$$g(u_i, v_i) = \beta u_i - u_i^2 v_i$$
$$(u^\star, v^\star) = (\alpha, \frac{\beta}{\alpha})$$

As desired, $g_v < 0 < f_u$ for our choice of α and β.

We initialize (D_u, D_v) such that $\text{Re}(\lambda_\alpha)_{\max} = 0$ for an arbitrary starting value of D_u (here we start with $D_u = 0.01$). Defining σ as before, our goal in doing this is to initialize $\sigma = \sigma_c$. We calculate $\sigma > \sigma_c$ such that $\Lambda_{c_2} - \Lambda_{c_1} = |\Lambda_0|$. This creates a Laplacian eigenvalue instability region with width equal to the spectral radius of L. We then choose D_u such that $\Lambda_{c_1} > -\Lambda_\alpha$ for all α, re-calculating $D_v = \sigma D_u$. More precisely, we choose D_u such that $\Lambda_{c_1} = -\Lambda_0 + 1$, so the leading eigenvalue is just shy of the Turing instability threshold, with instability region from $-\Lambda_0 + 1$ to $-2\Lambda_0 + 1$. We now have a pattern-enabled system $S \in \mathcal{S}_p$.

Procedural Variables: We start by setting the weight-collapse threshold $\theta = 0.5$. We choose δ-shifts such that $-(\Lambda_\tau + \delta_\tau) = \frac{1}{2}(\Lambda_{c_1} + \Lambda_{c_2})$, placing the now unstable target mode in the middle of the instability region before conducting the transformation $L_c \to L_f$.

---

[2]The ring lattice can be seen as a special case of a WS graph in which the re-wiring probability is 0.

Evaluation Criteria: To evaluate the success of the proposed control mechanism, we consider both a binary criterion (whether *only* the target mode has been destabilized) and two empirical measures (how far non-target eigenvalues deviate from their initial values and how many edge-changes are needed to go from L to L_f). We define the first empirical measure as the average percentage change of non-target eigenvalues, denoted by $\langle \rho \rangle$. The second, denoted ε, is defined as the number of nonzero elements of $A - A_f$, where A and A_f represent the adjacency matrices recovered from L and L_f respectively. We seek to understand the conditions for which any choice of τ satisfies the binary criterion, as well as those for which our empirical measures are minimized.

5.2.2 Results

For the binary success criterion, while $L \to L_f$ does not universally succeed in destabilizing some target mode τ, we do have high degrees of success across the domain of τ for certain graphs (see Table 5.1). In failure cases, we observe that we either fail to destabilize ($-\Lambda_\tau^{(f)} < \Lambda_{c_1}$), or some additional mode s is destabilized such that $\Lambda_{c_1} < -\Lambda_s^{(f)} < -\Lambda_\tau^{(f)} < \Lambda_{c_2}$. While we did not observe the case for which τ remained stable by overshooting the instability region (i.e. $-\Lambda_\tau^{(f)} > \Lambda_{c_2}$), we conjecture that it could be possible, potentially by choosing a set of pattern-enabled system parameters with an arbitrarily narrow instability region as well as a large δ_τ. As a final general observation, the binary criterion was more frequently satisfied for Λ_τ close to the instability threshold, consistent with the intuitive expectation that it is harder to de-stabilize modes further in the stability region.

Comparing results across graph types with equal average degree, we observe the success rate for the binary criterion is highest for WS graphs with low rewiring probability ($p = 0.1, 0.2$). ER graphs stand out as those with high variability for success relative to other graph models. BA graphs are exceptionally resilient against this control mechanism, with an average success rate of just 0.16%. Though a large number of edge-changes do occur across all τ values, our control mechanism hardly alters the original Laplacian spectrum of BA graphs, with a general trend indicating an increase in ρ as τ increases. See Appendix A for further details and sample results for each graph generation model.

As stated in Corollary 4.1.2, we remember that graphs with eigenvectors that demonstrate a high degree of localization can strongly influence the intermediate weighting as we transform from $L \to L_f$. As shown in [18] and supplemented by our simulated IPR calculations (see Appendix A), BA graphs display a substantially

Graph	Mean	Standard Deviation
Ring Lattice	92.93	0
BA	0.16	0.40
ER	82.01	9.08
WS ($p = 0.1$)	97.52	1.68
WS ($p = 0.2$)	93.47	3.07
WS ($p = 0.3$)	91.55	3.23
WS ($p = 0.4$)	91.11	4.76
WS ($p = 0.5$)	91.55	3.69
WS ($p = 0.6$)	90.78	4.75
WS ($p = 0.7$)	89.73	5.18
WS ($p = 0.8$)	90.30	4.95
WS ($p = 0.9$)	90.77	3.64

Table 5.1: **Binary Success Results** — Percentage of target eigenvalues fulfilling the binary criterion for various generation models for $N = 100, \langle k \rangle = 50$. Expressed as a mean and standard deviation over 100 simulations.

stronger degree of localization than other tested models. The stark contrast in success and resilience to our control mechanism for BA graphs may be explained in part by this localization, though further experimentation is needed to rigorously evaluate this hypothesis.

We now pay special attention to the case of the ring lattice. Looking at our empirical measures, as shown in Figures 5.3 and 5.2, we observe the number of edge changes generally increases as δ_τ increases, but with patches of deviation that depend on $\langle k \rangle$. While the dependence on $\langle k \rangle$ and the nature of deviation patches is unclear, the data otherwise appears to follow the shape of a logit function. The trend for the average percentage change does not demonstrate any statistically significant linear correlations as evaluated by Pearson's correlation coefficient, indicating τ may have less impact on this metric for the ring lattice.

(a) $\langle k \rangle = 40$ (b) $\langle k \rangle = 50$ (c) $\langle k \rangle = 60$
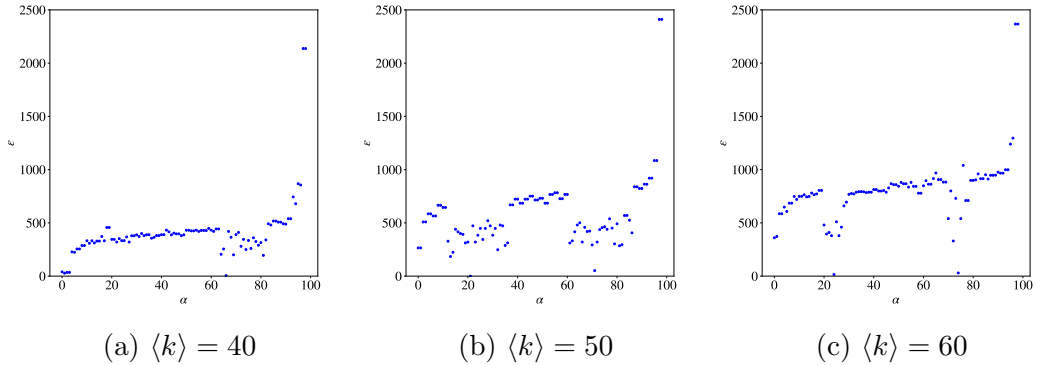
Figure 5.2: ε **vs. Target Index** — Results for ring lattice, $N = 100$

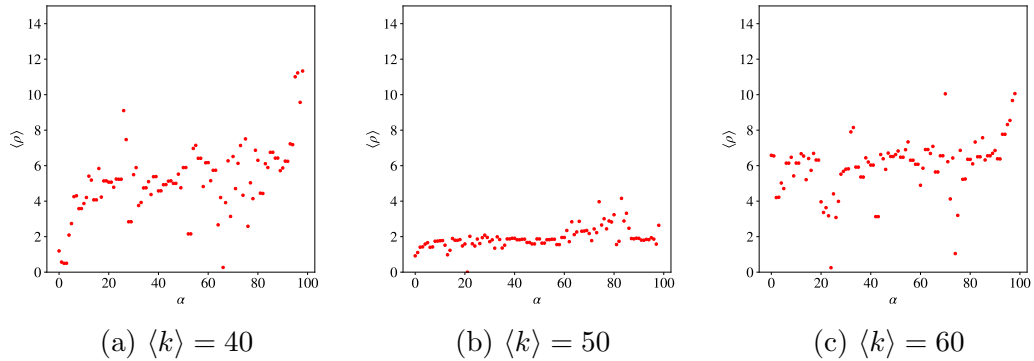(a) $\langle k \rangle = 40$ (b) $\langle k \rangle = 50$ (c) $\langle k \rangle = 60$

Figure 5.3: $\langle \rho \rangle$ **vs. Target Index** — Results for ring lattice, $N = 100$

Repeating simulations on variable numbers of nodes, we observe there appears to be a critical number of nodes above which $L \to L_f$ does not result in any structural changes (i.e. $L_f = L$). Moreover, we found that small θ corresponded to a higher number of non-edges being converted to edges, while large θ corresponded to higher number of edges being deleted. Though the number of edge changes generally appears to scale with τ, the net change in total degree does not, suggesting the structural changes occurring can largely be conceptualized as re-wiring. Additionally, the edge-changes demonstrate a high degree of symmetricity. Sample results are shown in Figure 5.4, where $\Delta|E|$ denotes the change in edge count between $\mathbf{G}$ and $\mathbf{G}_f$.

5.3   Theoretical Bounds

In light of numerical results, we develop theoretical expectations for $L \to L_f$ when $\mathbf{G}$ is a ring lattice.

25

(a)
$\tau = 0$
$\Delta|E| +21$

(b)
$\tau = 2$
$\Delta|E| +23$

(c)
$\tau = 50$
$\Delta|E| +17$
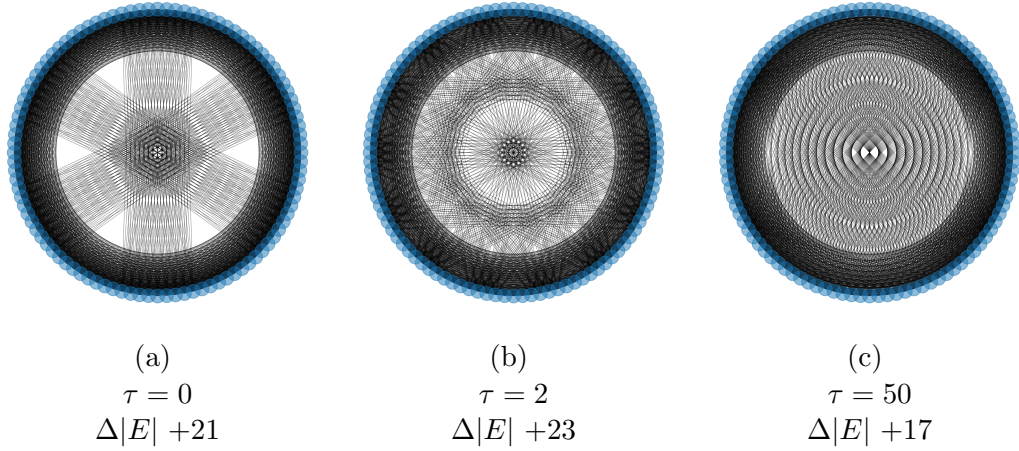
Figure 5.4: **Symmetric Re-wiring** — Visualizations of $\mathbf{G}_f$ for variable τ when $\mathbf{G}$ is a ring lattice and $N = 100, \langle k \rangle = 50$. Additional examples in Appendix B.

Theorem 5.3.1. *For $\mathbf{G}$ a ring lattice and a target mode τ, $\left| \eta^{(\tau)}(i,j) \right| \leq \frac{2}{N} |\delta_\tau|$*

Proof.

$$L_{ring} = \begin{pmatrix} c_0 & c_1 & c_2 & \dots & \dots & c_{n-1} \\ c_{n-1} & c_0 & c_1 & c_2 & \dots & c_{n-2} \\ \vdots & c_{n-1} & c_0 & c_1 & \ddots & \vdots \\ & & \ddots & \ddots & \ddots & \vdots \\ & & & & & c_1 \\ c_1 & \dots & \dots & \ddots & c_{n-1} & c_0 \end{pmatrix}$$

Observe that the Laplacian for a ring lattice is a circulant matrix. We therefore know its spectrum[3] and eigenvectors in terms of the first row of L_{ring}.

$$\Lambda_\alpha = \sum_{k=0}^{N-1} c_k e^{\frac{2\pi \imath \alpha}{N} k}$$

$$\phi_j^{(\alpha)} = \frac{1}{\sqrt{N}} (e^{\frac{2\pi \imath \alpha}{N} j})$$

From this complex eigenbasis, we can derive a real eigenbasis. Namely, for all α, we seek to generate a new eigenvector $\omega^{(\alpha)} \in \mathbb{R}^N$ from $\phi^{(\alpha)} \in \mathbb{C}^N$. Observe that for some complex eigenvector ν, at least one of the following statements is true:

1. $\nu + \bar{\nu} = 2\text{Re}(\nu)$ is an eigenvector

2. $\imath(\nu - \bar{\nu}) = -2\text{Im}(\nu)$ is an eigenvector

---

[3]The spectrum can also be seen as a discrete Fourier transform (DFT) of the first row.

26

Statements (1) and (2) are respectively false when $\text{Re}(\nu)$ and $\text{Im}(\nu)$ are the 0 vector. When both are false, ν must be the 0 vector, which leads to a contradiction, as the 0 vector is not an eigenvector. Therefore, at least one of (1) and (2) is true.

In our case, $\text{Re}(\phi_j^{(\alpha)}) = \frac{1}{\sqrt{N}}\left[\cos(\frac{2\pi\alpha}{N}j)\right]$ and $\text{Im}(\phi_j^{(\alpha)}) = \frac{1}{\sqrt{N}}\left[\sin(\frac{2\pi\alpha}{N}j)\right]$. We first ask what happens if we use statement (1) to form real eigenvectors from the real component of $\phi^{(\alpha)}$. Cosine is an even function, so when $\alpha + \beta = N$, $\omega^{(\alpha)} = \omega^{(\beta)}$. Statement (1) therefore only helps us generate a set of $\frac{N}{2}+1$ unique real eigenvectors for even N and $\frac{N+1}{2}$ for odd N. Statement (2), on the other hand, avoids this symmetry issue, but produces the 0 vector for $\alpha = 0$, and, for even N, $\alpha = \frac{N}{2}$. For these cases[4] we can leverage statement (1) to produce unique nonzero eigenvectors. After normalizing, we achieve the final set

$$
\omega_j^{(\alpha)} = \begin{cases} \dfrac{-2}{\sqrt{2N}}\sin(\dfrac{2\pi\alpha}{N}j) \text{ if } \alpha \notin \{0, \dfrac{N}{2}\} \\[3mm] \dfrac{1}{\sqrt{N}}\cos(\dfrac{2\pi\alpha}{N}j) \text{ if } \alpha \in \{0, \dfrac{N}{2}\} \end{cases} \quad \text{for } \alpha = 0, 1, \ldots, N-1
$$

We can now plug into $\eta^{(\tau)}(i,j)$ and consider its maximum.

Case 1: $\tau \notin \{0, \frac{N}{2}\}$

$$
\begin{aligned}
\max\left|\eta^{(\tau)}(i,j)\right| &= \max\left|\frac{2}{N}\sin\left(\frac{2\pi\tau}{N}i\right)\sin\left(\frac{2\pi\tau}{N}j\right)\right||\delta_\tau| \\
&= \max\left|\frac{1}{N}\left[\cos\left(\frac{2\pi\tau}{N}(i-j)\right) - \cos\left(\frac{2\pi\tau}{N}(i+j)\right)\right]\right||\delta_\tau| \\
&\leq \boxed{\frac{2}{N}|\delta_\tau|}
\end{aligned}
$$

Case 2: $\tau \in \{0, \frac{N}{2}\}$

$$
\begin{aligned}
\max\left|\eta^{(\tau)}(i,j)\right| &= \max\left|\frac{1}{N}\cos\left(\frac{2\pi\tau}{N}i\right)\cos\left(\frac{2\pi\tau}{N}j\right)\right||\delta_\tau| \\
&= \max\left|\frac{1}{2N}\left[\cos\left(\frac{2\pi\tau}{N}(i-j)\right) + \cos\left(\frac{2\pi\tau}{N}(i+j)\right)\right]\right||\delta_\tau| \\
&\leq \boxed{\frac{1}{N}|\delta_\tau|}
\end{aligned}
$$

We have thus proved an upper bound: $\left|\eta^{(\tau)}(i,j)\right| \leq \frac{2}{N}|\delta_\tau|$. $\qquad\qquad\square$

---

[4]Noting that $\frac{N}{2}$ is not in the domain of α for odd N, we henceforth collectively treat the 0-vector cases as the cases in which $\alpha \in \{0, \frac{N}{2}\}$ without loss of generality

Theorem 5.3.1 is consistent with empirical results as well. Having identified an upper bound on $\left|\eta^{(\tau)}(i,j)\right|$, we can further contextualize scenarios in which $L_f = L$. For a chosen τ, let $\widetilde{\eta}(\tau)$ denote the actual maximum achieved by $\left|\eta^{(\tau)}(i,j)\right|$ over all (i,j) pairs (as opposed to just an upper bound). If

$$\widetilde{\eta}(\tau) < \theta \implies (L_f)_{ij} = L_{ij}, \forall L_{ij} = 0$$
$$\widetilde{\eta}(\tau) < 1 - \theta \implies (L_f)_{ij} = L_{ij}, \forall L_{ij} = -1$$

We have identified separate conditions for which all non-edges remain non-edges and all edges remain edges. When both conditions are satisfied, the weight-collapse function essentially restores L_c to L, resulting in $L_f = L$. This logic similarly supports results indicating that decreasing θ lowered the threshold for edge addition, while increasing θ lowered the threshold for edge deletion.

Corollary 5.3.1. *For* **G** *a ring lattice, if* $\lim_{N \to \infty} \frac{|\delta_\tau|}{N} = 0$, *then there exists some critical number of nodes, N_c, above which $L \to L_f$ results in $L = L_f$ for a given target and constant $\langle k \rangle$.*

The conditional statement is necessary because our choice of N impacts the upper bound of $\widetilde{\eta}(\tau)$ in two ways. We see directly an upper bound dependence on N^{-1}, but there is an additional dependence of $|\delta_\tau|$ on N. Our problem set-up requires us to choose δ-shifts that push eigenvalues into the instability region, which we calculate using the gap between the lower threshold (as determined by Λ_0) and Λ_τ. Since the spectrum of L depends on N (and $\langle k \rangle$), and δ_τ depends on the spectrum, δ_τ depends on N. If N grows faster than $|\delta_\tau|$ for increasing N, the maximum possible value of $\widetilde{\eta}(\tau)$ (identified in Theorem 5.3.1) is driven smaller and smaller, until eventually $\widetilde{\eta}(\tau) < \theta$ and $\widetilde{\eta}(\tau) < 1 - \theta$ are both necessarily true; no edge-changes occur in this transformation. More precisely, we define

$$N_c = \inf\{N : \widetilde{\eta}(\tau) < \min\{\theta, 1 - \theta\}\}$$

Proposition 5.3.1. *For* **G** *a ring lattice, $\lim_{N \to \infty} \frac{|\delta_\tau|}{N} = 0$ is always true for constant $\langle k \rangle$.*

Proof. We prove Proposition 5.3.1 by directly considering $\lim_{N \to \infty} \frac{|\delta_\tau|}{N}$. We note that the maximum δ-shift will always be δ_F given our problem set-up, where δ_F corresponds to the Fiedler eigenvalue Λ_F. Since shifts are ordered, to prove the limit for all τ, it is sufficient to prove $\lim_{N \to \infty} \frac{|\delta_\tau|}{N} = 0$ holds for δ_F. We now consider an upper bound on $|\delta_F|$ in terms of N and $\langle k \rangle$. Our scheme dictates δ_τ such that $-(\Lambda_\tau + \delta_\tau) = \frac{1}{2}(\Lambda_{c_1} + \Lambda_{c_2})$,

which we can re-write in terms of the leading eigenvector: $-(\Lambda_\tau + \delta_\tau) = \frac{1}{2}(-3\Lambda_0 + 2)$. Therefore

$$|\delta_F| = \frac{3}{2}|\Lambda_0| - |\Lambda_F| + 1$$

We can put an upper bound on $|\delta_F|$ by using a bound from above for $|\Lambda_0|$ and a bound from below for $|\Lambda_F|$. Namely, via the Perron-Frobenius theorem, $|\Lambda_0| \le k_{max} = \langle k \rangle$. From [28], we have $4(N\mathcal{D})^{-1} \le |\Lambda_F|$, where $\mathcal{D}$ is the diameter of the network. For the ring lattice, we minimize the lower bound on $|\Lambda_F|$ with a maximum possible $\mathcal{D}$ of $\frac{N}{2}$, implying $8N^{-2} \le |\Lambda_F|$. We now have an upper bound on $|\delta_F|$.

$$|\delta_F| \le \frac{3}{2}\langle k \rangle - 8N^{-2} + 1$$

It will be sufficient to assume the equality case for maximal $|\delta_F|$, which we plug into our limit of interest.

$$\lim_{N \to \infty} \frac{|\delta_F|}{N} = \lim_{N \to \infty} \left(\frac{3\langle k \rangle}{2N} - \frac{8}{N^3} + \frac{1}{N} \right)$$

For constant $\langle k \rangle$, this limit evaluates to 0. We have thus proved $\lim_{N \to \infty} \frac{|\delta_F|}{N} = 0$, which is sufficient to prove $\lim_{N \to \infty} \frac{|\delta_\tau|}{N} = 0$. $\square$

Because $\lim_{N \to \infty} \frac{|\delta_\tau|}{N} = 0$ is true for the ring lattice, we can assume the existence of N_c. This theoretical result is consistent with the critical number of nodes observed in the numerical simulations, above which $L_f = L$.

Corollary 5.3.2. *N must be even for* $\widetilde{\eta}(\tau) = \frac{2}{N}|\delta_\tau|$

The frequency with which $\left| \eta^{(\tau)}(i, j) \right|$ reaches its maximum value $\widetilde{\eta}(\tau)$ over all (i, j) pairs depends on N, τ. When $\widetilde{\eta}(\tau)$ is $\frac{2}{N}|\delta_\tau|$, we require $\tau \notin \{0, \frac{N}{2}\}$ and one of two possible scenarios:

Case 1: $\cos\left(\frac{2\pi\tau}{N}(i - j)\right) - \cos\left(\frac{2\pi\tau}{N}(i + j)\right) = 2$

The argument of the first cosine term must be an integer multiple of 2π, while the argument of the second is an integer multiple of 2π shifted by π.

$$\frac{2\pi\tau}{N}(i - j) = 2\pi\kappa_1$$
$$\frac{2\pi\tau}{N}(i + j) = \pi + 2\pi\kappa_2$$
$$\kappa_1, \kappa_2 \in \mathbb{Z}_+$$

We therefore have $\tau(i-j) = N\kappa_1$ and $\tau(i+j) = \frac{N}{2} + N\kappa_2$.

Case 2: $\cos\left(\frac{2\pi\tau}{N}(i-j)\right) - \cos\left(\frac{2\pi\tau}{N}(i+j)\right) = -2$

The argument of the second cosine term must be an integer multiple of 2π, while the argument of the first is an integer multiple of 2π shifted by π.

$$\frac{2\pi\tau}{N}(i-j) = \pi + 2\pi\kappa_1$$
$$\frac{2\pi\tau}{N}(i+j) = 2\pi\kappa_2$$
$$\kappa_1, \kappa_2 \in \mathbb{Z}_+$$

We therefore have $\tau(i-j) = \frac{N}{2} + N\kappa_1$ and $\tau(i+j) = N\kappa_2$.

As τ, i, j are all integers, $\tau(i \pm j)$ is an integer as well, so we need $\frac{N}{2}$ to be an integer. Both cases therefore require even N for $\widetilde{\eta}(\tau)$ to reach its upper bound.

Proposition 5.3.2. *Assume there exists some set of N, denoted $\mathbf{N}^\star$, for which $\tau \in \{0, \frac{N}{2}\}$ guarantees $L = L_f$, while $\tau \notin \{0, \frac{N}{2}\}$ does not. For the special case of $\theta = 1 - \theta = 0.5$, $\mathbf{N}^\star = \emptyset$ iff $|\Lambda_F| \leq \frac{|\Lambda_0|}{2} - 1$.*

As a final note, we propose results following from the differing upper bounds of $\left|\eta^{(\tau)}(i,j)\right|$ for $\tau \in \{0, \frac{N}{2}\}$ and $\tau \notin \{0, \frac{N}{2}\}$. We prove Proposition 5.3.2 by first assuming $\mathbf{N}^\star$ is nonempty and attempt to construct its elements.

Here we define $\mathbf{N}^\star$:

$$\mathbf{N}_\tau = \{N : 2\,|\delta_\tau| < N < 4\,|\delta_\tau|\}$$
$$\mathbf{N}^\star = \bigcap_\tau \mathbf{N}_\tau$$

$\mathbf{N}_\tau$ is directly obtained by requiring 1) $\frac{1}{N}\,|\delta_\tau| < \frac{1}{2}$ and 2) $\frac{2}{N}\,|\delta_\tau| > \frac{1}{2}$. Condition 1) restricts N to the set of values that guarantees $\max\left|\eta^{(\tau)}(i,j)\right| < \min\{\theta, 1 - \theta\}$ for $\tau \in \{0, \frac{N}{2}\}$. Condition 2) imposes the restriction that each element of $\mathbf{N}^\star$ is less than N_c; otherwise, we would allow values of N for which $L = L_f$ for all τ. We therefore define a set indexed by τ which includes values of N for which 1) and 2) hold for a given τ, then define $\mathbf{N}^\star$ as the intersection of these sets. Because our δ shifts are ordered, we can bypass this two-step process by directly considering the maximum and minimum possible values of $2\,|\delta_\tau|$ and $4\,|\delta_\tau|$ respectively.

$$\mathbf{N}^\star = \{N : 2\max_\tau\,|\delta_\tau| < N < 4\min_\tau\,|\delta_\tau|\}$$

We can re-write the set condition statement as follows.

$$2 \max_{\tau} |\delta_\tau| < N < 4 \min_{\tau} |\delta_\tau|$$
$$2 |\delta_F| < N < 4 |\delta_0|$$

Plugging in from our procedure, we get

$$3 |\Lambda_0| + 2 - 2 |\Lambda_F| < N < 2 |\Lambda_0| + 4 \qquad (5.1)$$

We now directly compare the least and greatest terms of the inequality above.

$$3 |\Lambda_0| + 2 - 2 |\Lambda_F| < 2 |\Lambda_0| + 4$$
$$|\Lambda_F| > \frac{|\Lambda_0|}{2} - 1$$

When $|\Lambda_F| \leq \frac{|\Lambda_0|}{2} - 1$, it is impossible for some N to exist where Inequality 5.1 is true. As there is no such N that fits the criteria, $\mathbf{N}^\star = \emptyset$. This condition describes the gap between the leading and Fiedler eigenvalues and is generally easy to fulfill on random networks, as breaking it requires a very small number of nodes alongside a low average degree. In our numerical simulations, the condition $|\Lambda_F| \leq \frac{|\Lambda_0|}{2} - 1$ was always fulfilled, and we accordingly observed $\mathbf{N}^\star = \emptyset$.

Chapter 6

Conclusion

In addition to rigorously developing fundamentals of network Turing patterns, our work analyzes a new topological control mechanism for targeted mode destabilization, building a deeper theoretical understanding of structurally mediated Turing patterns. There are a number of related research questions spawning from these results. For instance, existing topological control studies typically "draw their conclusions by comparing two different static network topologies" [40]. Such is the case in our work, as we treat the control intervention as a discrete shift from one static architecture (L) to another (L_f). Applying this work to temporal networks, whose topologies can change over continuous time, could prove to be a promising research space. Furthermore, given the stark difference in success for networks with varying degrees of Laplacian eigenvector localization, future studies might seek to understand the relationship between degree heterogeneity, localization, and pattern emergence. Though we pay special attention to the ring lattice, there are further unexplored directions for this graph type, such as quantifying pattern invariance when destabilizing different targets. Lastly, attempting to prove boundedness results similar to Theorem 5.3.1 on random graphs could prove a fruitful endeavor as well. Ultimately, this work seeks to enhance our theoretical understanding of pattern formation in light of the omnipresent and salient real-world examples of reaction-diffusion systems on networks.

Appendix

A: Supplementary Results from Numerical Simulations

(a) ε **vs. Target Index** — Results for $N = 100, \langle k \rangle = 50$

(b) $\langle \rho \rangle$ **vs. Target Index** — Results for $N = 100, \langle k \rangle = 50$
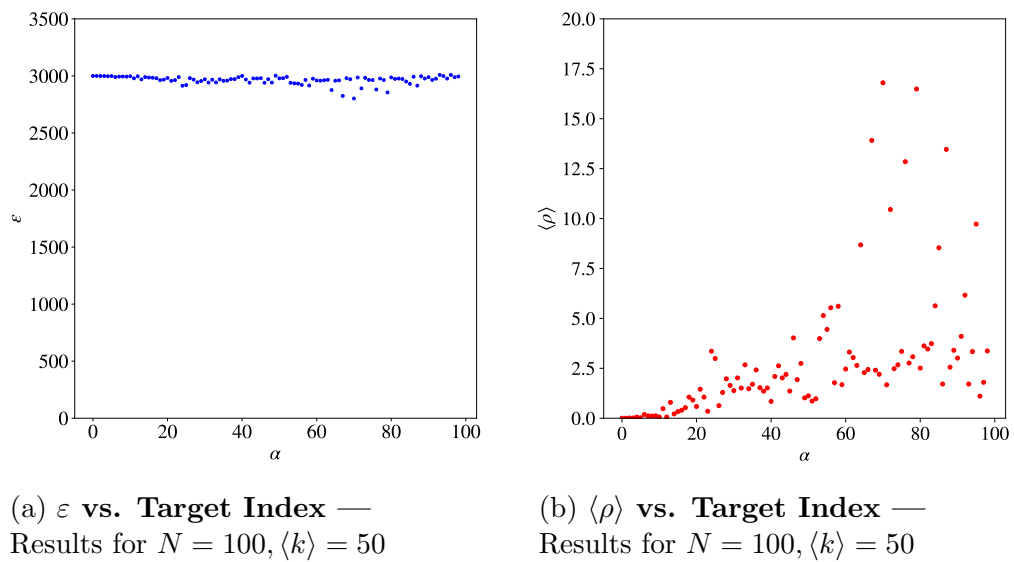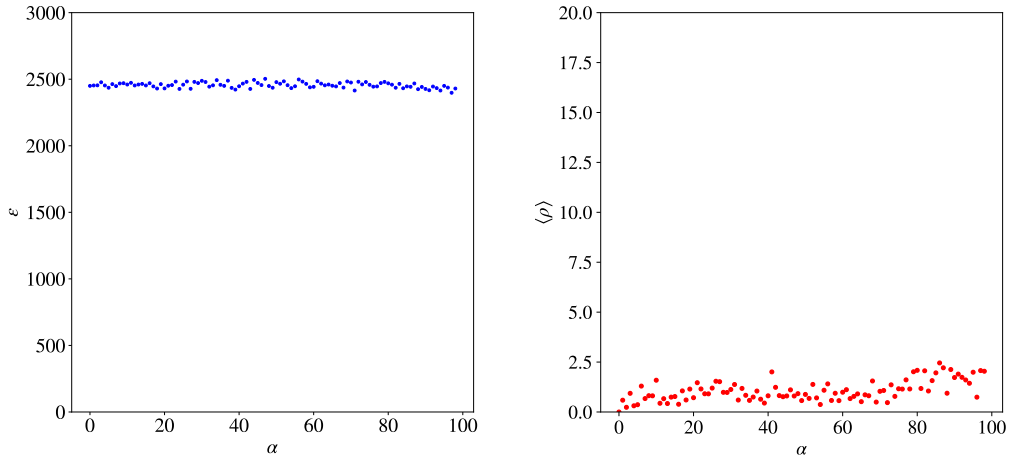
Figure 1: BA Model averaged over 100 runs

(a) ε **vs. Target Index** — Results for $N = 100, \langle k \rangle = 50$

(b) $\langle \rho \rangle$ **vs. Target Index** — Results for $N = 100, \langle k \rangle = 50$
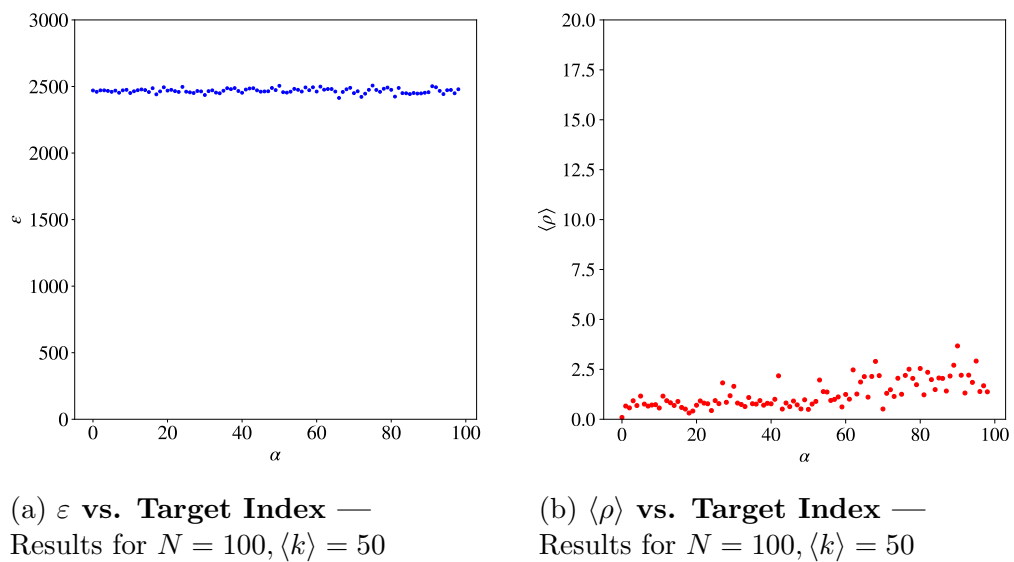
Figure 2: ER Model averaged over 100 runs
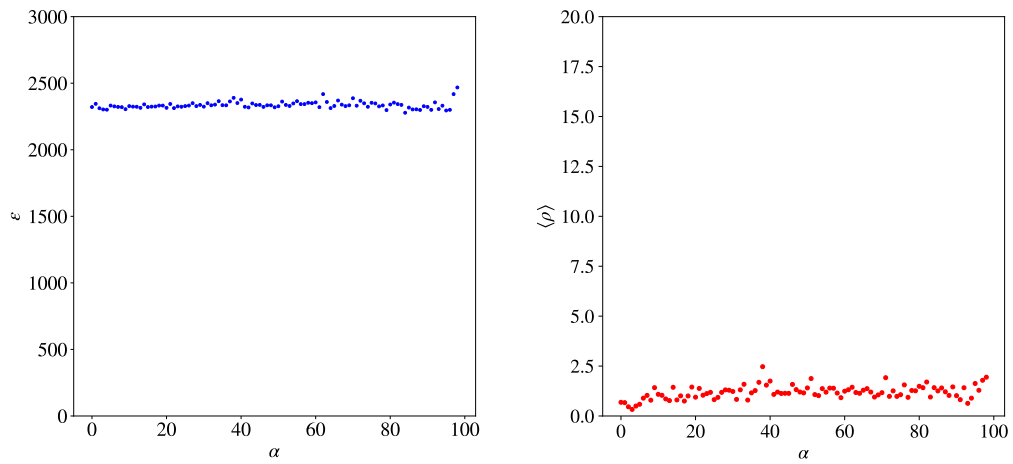
(a) ε **vs. Target Index** — Results for $N = 100, \langle k \rangle = 50$

(b) $\langle \rho \rangle$ **vs. Target Index** — Results for $N = 100, \langle k \rangle = 50$

Figure 3: WS Model averaged over 100 runs, $p = 0.1$
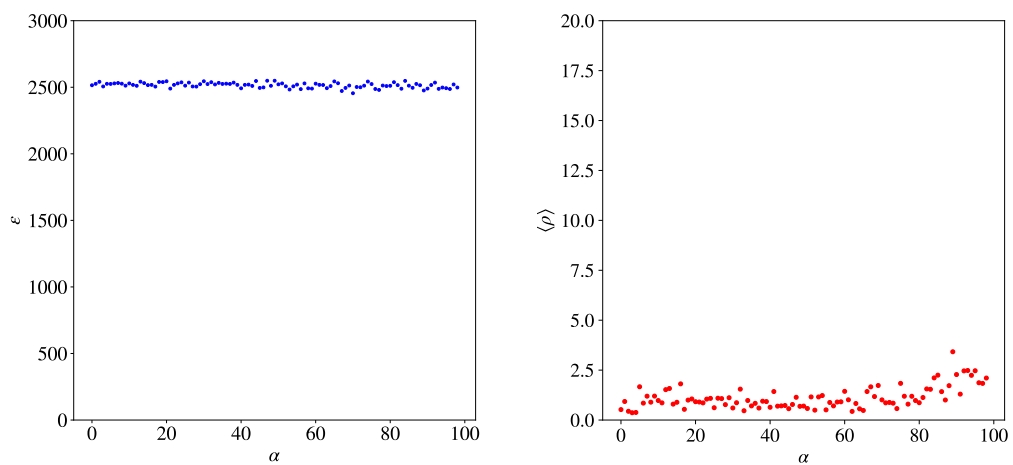
(a) ε **vs. Target Index** — Results for $N = 100, \langle k \rangle = 50$

(b) $\langle \rho \rangle$ **vs. Target Index** — Results for $N = 100, \langle k \rangle = 50$

Figure 4: WS Model averaged over 100 runs, $p = 0.5$

(a) ε **vs. Target Index** — Results for $N = 100, \langle k \rangle = 50$

(b) $\langle \rho \rangle$ **vs. Target Index** — Results for $N = 100, \langle k \rangle = 50$

Figure 5: WS Model averaged over 100 runs, $p = 0.9$

Graph	Mean
Ring Lattice	0.054
BA	0.417
ER	0.049
WS ($p = 0.1$)	0.059
WS ($p = 0.5$)	0.041
WS ($p = 0.9$)	0.046

Table 1: **IPR Scores** — Average localization score across all eigenvectors for various models when $N = 100, \langle k \rangle = 50$.
Expressed as a mean over 100 simulations.

B: Symmetric Re-wiring
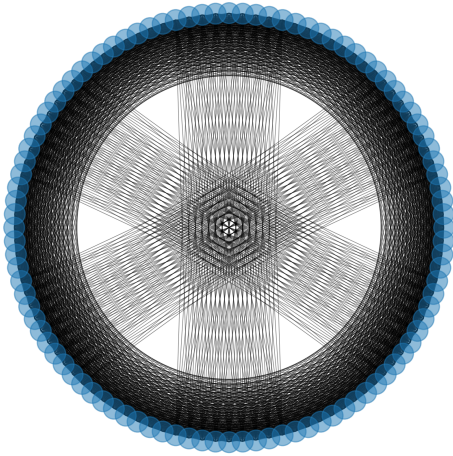
(a) $\Lambda_\tau = \Lambda_0$
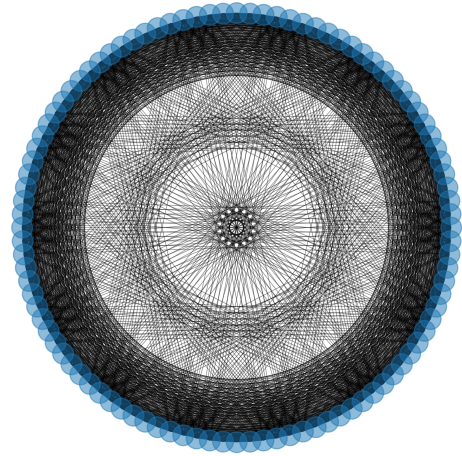
(b) $\Lambda_\tau = \Lambda_2$
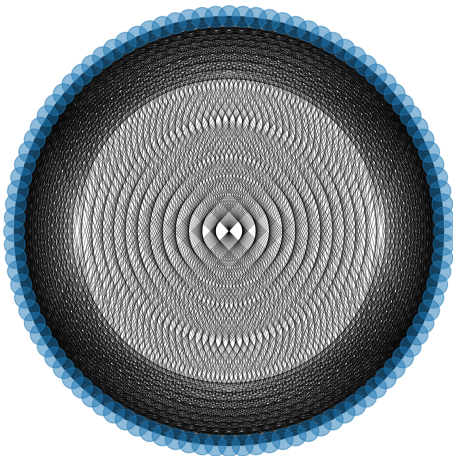
(c) $\Lambda_\tau = \Lambda_{49}$
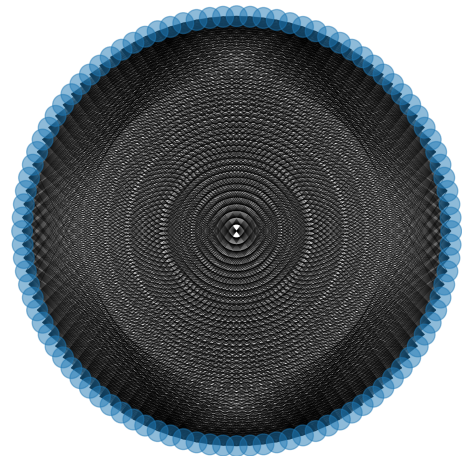
(d) $\Lambda_\tau = \Lambda_{98}$

Figure 6: $\mathbf{G}_f$ — Visualization of $\mathbf{G}_f$ for changing τ when $\mathbf{G}$ is a ring lattice on $N = 100, \langle k \rangle = 50$.

C: Emergence of Patterns in Network Reaction-Diffusion System
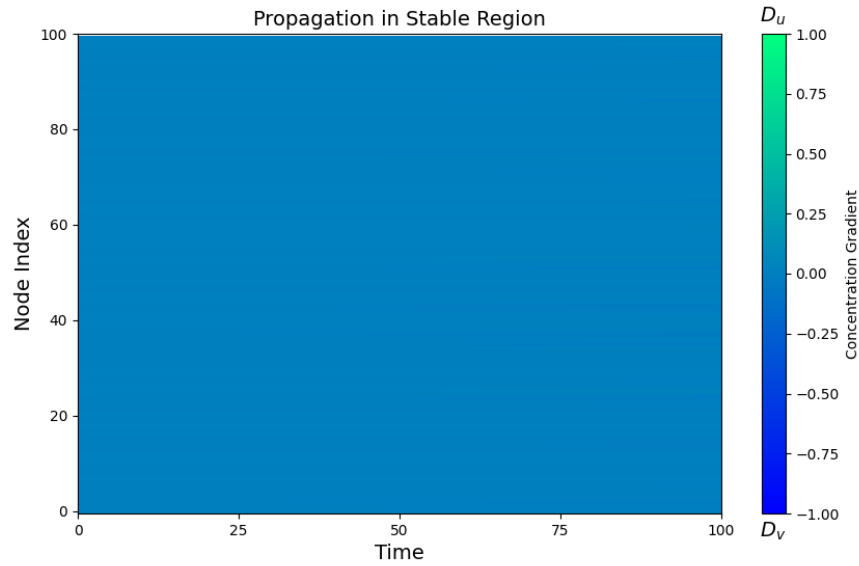
(a) No pattern formation in stable system
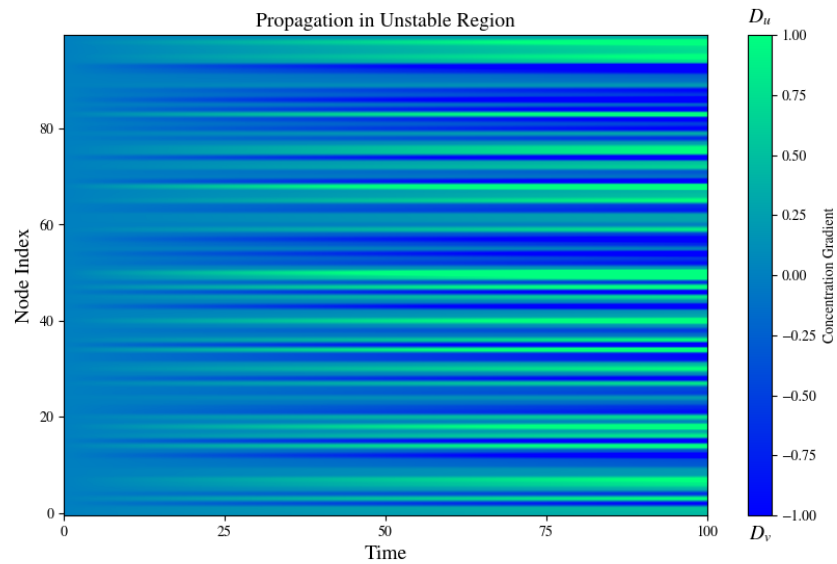
(b) Pattern formation in unstable system

Figure 7: **Propagation Results** — Concentration of diffusive species by node after perturbing the initial uniform distribution of the activator-inhibitor system

Bibliography

[1] Igor S. Aranson and Lorenz Kramer. The world of the complex Ginzburg-Landau equation. *Reviews of Modern Physics*, 74(1):99–143, February 2002. Publisher: American Physical Society. URL: `https://link.aps.org/doi/10.1103/RevModPhys.74.99`, `doi:10.1103/RevModPhys.74.99`.

[2] Malbor Asllani, Daniel M. Busiello, Timoteo Carletti, Duccio Fanelli, and Gwendoline Planchon. Turing patterns in multiplex networks. *Physical Review E*, 90(4):042814, October 2014. Publisher: American Physical Society. URL: `https://link.aps.org/doi/10.1103/PhysRevE.90.042814`, `doi:10.1103/PhysRevE.90.042814`.

[3] Malbor Asllani, Timoteo Carletti, and Duccio Fanelli. Tune the topology to create or destroy patterns. *The European physical journal. B, Condensed matter physics*, 89(12):1–10, 2016. Place: Berlin/Heidelberg Publisher: Springer Berlin Heidelberg. `doi:10.1140/epjb/e2016-70248-6`.

[4] Malbor Asllani, Joseph D. Challenger, Francesco Saverio Pavone, Leonardo Sacconi, and Duccio Fanelli. The theory of pattern formation on directed networks. *Nature Communications*, 5(1):4517, July 2014. Number: 1 Publisher: Nature Publishing Group. URL: `https://www.nature.com/articles/ncomms5517`, `doi:10.1038/ncomms5517`.

[5] Philip Ball. Forging patterns and making waves from biology to geology: a commentary on Turing (1952) 'The chemical basis of morphogenesis'. *Philosophical Transactions of the Royal Society B: Biological Sciences*, 370(1666):20140218, April 2015. Publisher: Royal Society. URL: `https://royalsocietypublishing.org/doi/full/10.1098/rstb.2014.0218`, `doi:10.1098/rstb.2014.0218`.

[6] Timoteo Carletti, Malbor Asllani, Duccio Fanelli, and Vito Latora. Nonlinear walkers and efficient exploration of congested networks. *Physical Review Research*, 2(3):033012, July 2020. URL: https://link.aps.org/doi/10.1103/PhysRevResearch.2.033012, doi:10.1103/PhysRevResearch.2.033012.

[7] JULYAN H. E. Cartwright. Labyrinthine Turing Pattern Formation in the Cerebral Cortex. *Journal of Theoretical Biology*, 217(1):97–103, July 2002. URL: https://www.sciencedirect.com/science/article/pii/S0022519302930122, doi:10.1006/jtbi.2002.3012.

[8] Giulia Cencetti, Franco Bagnoli, Giorgio Battistelli, Luigi Chisci, Francesca Di Patti, and Duccio Fanelli. Topological stabilization for synchronized dynamics on networks. *The European physical journal. B, Condensed matter physics*, 90(1):1–14, 2017. Place: Berlin/Heidelberg Publisher: Springer Berlin Heidelberg. doi:10.1140/epjb/e2016-70465-y.

[9] Giulia Cencetti, Pau Clusella, and Duccio Fanelli. Pattern invariance for reaction-diffusion systems on complex networks. *Scientific Reports*, 8(1):16226, November 2018. Number: 1 Publisher: Nature Publishing Group. URL: https://www.nature.com/articles/s41598-018-34372-0, doi:10.1038/s41598-018-34372-0.

[10] Giulia Cencetti, Pau Clusella, and Duccio Fanelli. SUPPLEMENT: Pattern invariance for reaction-diffusion systems on complex networks. *Scientific Reports*, 8(1):16226, November 2018. URL: https://www.nature.com/articles/s41598-018-34372-0, doi:10.1038/s41598-018-34372-0.

[11] Vittoria Colizza, Alessandro Vespignani, and Romualdo Pastor-Satorras. Reaction-diffusion processes and metapopulation models in heterogeneous networks. *Nature physics*, 3(4):276–282, 2007. Place: London Publisher: Nature Publishing Group. doi:10.1038/nphys560.

[12] Xavier Diego, Luciano Marcon, Patrick Müller, and James Sharpe. Key Features of Turing Systems are Determined Purely by Network Topology. *Physical review. X*, 8(2):021071–, 2018. Place: College Park Publisher: American Physical Society. doi:10.1103/PhysRevX.8.021071.

[13] Moran Duan, Lili Chang, and Zhen Jin. Turing patterns of an SI epidemic model with cross-diffusion on complex networks. *Physica A: Statistical Mechanics and its Applications*, 533:122023, November 2019. URL: https:

//www.sciencedirect.com/science/article/pii/S0378437119311598, `doi:`
`10.1016/j.physa.2019.122023`.

[14] Carles Falcó. From random walks on networks to nonlinear diffusion. *Physical Review E*, 106(5):054103, November 2022. arXiv:2206.08859 [physics]. URL: `http://arxiv.org/abs/2206.08859`, `doi:10.1103/PhysRevE.106.054103`.

[15] Yuki Fuseya, Hiroyasu Katsuno, Kamran Behnia, and Aharon Kapitulnik. Nanoscale Turing patterns in a bismuth monolayer. *Nature physics*, 17(9):1031–1036, 2021. Place: BERLIN Publisher: NATURE PORTFOLIO. `doi:10.1038/s41567-021-01288-y`.

[16] Michael C. Getz, Jasmine A. Nirody, and Padmini Rangamani. Stability analysis in spatial modeling of cell signaling. *WIREs Systems Biology and Medicine*, 10(1):e1395, January 2018. URL: `https://wires.onlinelibrary.wiley.com/doi/10.1002/wsbm.1395`, `doi:10.1002/wsbm.1395`.

[17] Valeria Giunta, Maria Carmela Lombardo, and Marco Sammartino. Pattern Formation and Transition to Chaos in a Chemotaxis Model of Acute Inflammation. *SIAM Journal on Applied Dynamical Systems*, 20(4):1844–1881, January 2021. URL: `https://epubs.siam.org/doi/10.1137/20M1358104`, `doi:10.1137/20M1358104`.

[18] Shigefumi Hata and Hiroya Nakao. Localization of Laplacian eigenvectors on random networks. *Scientific Reports*, 7(1):1121, April 2017. Number: 1 Publisher: Nature Publishing Group. URL: `https://www.nature.com/articles/s41598-017-01010-0`, `doi:10.1038/s41598-017-01010-0`.

[19] Yusuke Ide, Hirofumi Izuhara, and Takuya Machida. Turing instability in reaction–diffusion models on complex networks. *Physica A*, 457:331–347, 2016. Publisher: Elsevier B.V. `doi:10.1016/j.physa.2016.03.055`.

[20] C. Konow, M. Dolnik, and I. R. Epstein. Insights from chemical systems into Turing-type morphogenesis. *Philosophical Transactions of the Royal Society A: Mathematical, Physical and Engineering Sciences*, 379(2213):20200269, November 2021. Publisher: Royal Society. URL: `https://royalsocietypublishing.org/doi/full/10.1098/rsta.2020.0269`, `doi:10.1098/rsta.2020.0269`.

[21] Renaud Lambiotte. Continuous-Time Random Walks and Temporal Networks.

[22] Chen Liu, Lili Chang, Yue Huang, and Zhen Wang. Turing patterns in a predator–prey model on complex networks. *Nonlinear Dynamics*, 99(4):3313–3322, March 2020. URL: `http://link.springer.com/10.1007/s11071-019-05460-1`, `doi:10.1007/s11071-019-05460-1`.

[23] J.R. Lowney and R.D. Larrabee. The use of Fick's law in modeling diffusion processes. *IEEE Transactions on Electron Devices*, 27(9):1795–1798, September 1980. Conference Name: IEEE Transactions on Electron Devices. URL: `https://ieeexplore.ieee.org/abstract/document/1480898`, `doi:10.1109/T-ED.1980.20105`.

[24] Naoki Masuda, Mason A. Porter, and Renaud Lambiotte. Random walks and diffusion on networks. *Physics Reports*, 716-717:1–58, November 2017. URL: `https://www.sciencedirect.com/science/article/pii/S0370157317302946`, `doi:10.1016/j.physrep.2017.07.007`.

[25] Patrick N. McGraw and Michael Menzinger. Laplacian Spectra as a Diagnostic Tool for Network Structure and Dynamics. *Physical Review E*, 77(3):031102, March 2008. arXiv:0708.4206 [cond-mat]. URL: `http://arxiv.org/abs/0708.4206`, `doi:10.1103/PhysRevE.77.031102`.

[26] Sayat Mimar, Mariamo Mussa Juane, Juyong Park, Alberto P. Muñuzuri, and Gourab Ghoshal. Turing patterns mediated by network topology in homogeneous active systems. *Physical review. E*, 99(6-1):062303–062303, 2019. Place: United States Publisher: American Physical Society APS. `doi:10.1103/PhysRevE.99.062303`.

[27] M. Mimura and J.D. Murray. On a diffusive prey-predator model which exhibits patchiness. *Journal of Theoretical Biology*, 75(3):249–262, December 1978. URL: `https://linkinghub.elsevier.com/retrieve/pii/0022519378903326`, `doi:10.1016/0022-5193(78)90332-6`.

[28] Bojan Mohar, Ed Y Alavi, G Chartrand, O R Oellermann, and A J Schwenk. The Laplacian Spectrum of Graphs. *Graph theory, combinatorics, and applications*, 1991.

[29] Arnab Mondal, Ranjit Kumar Upadhyay, Argha Mondal, and Sanjeev Kumar Sharma. Emergence of Turing patterns and dynamic visualization in excitable neuron model. *Applied Mathematics and Computation*, 423:127010,

June 2022. URL: `https://www.sciencedirect.com/science/article/pii/S0096300322000960`, `doi:10.1016/j.amc.2022.127010`.

[30] Hiroya Nakao and Alexander S. Mikhailov. Turing patterns in network-organized activator–inhibitor systems. *Nature Physics*, 6(7):544–550, July 2010. URL: `https://www.nature.com/articles/nphys1651`, `doi:10.1038/nphys1651`.

[31] Romualdo Pastor-Satorras and Alessandro Vespignani. Epidemic Spreading in Scale-Free Networks. *Physical Review Letters*, 86(14):3200–3203, April 2001. Publisher: American Physical Society. URL: `https://link.aps.org/doi/10.1103/PhysRevLett.86.3200`, `doi:10.1103/PhysRevLett.86.3200`.

[32] B. Peña and C. Pérez-García. Stability of Turing patterns in the Brusselator model. *Physical Review E*, 64(5):056213, October 2001. Publisher: American Physical Society. URL: `https://link.aps.org/doi/10.1103/PhysRevE.64.056213`, `doi:10.1103/PhysRevE.64.056213`.

[33] Julien Petit, Ben Lauwens, Duccio Fanelli, and Timoteo Carletti. Theory of Turing Patterns on Time Varying Networks. *Physical Review Letters*, 119(14):148301, October 2017. Publisher: American Physical Society. URL: `https://link.aps.org/doi/10.1103/PhysRevLett.119.148301`, `doi:10.1103/PhysRevLett.119.148301`.

[34] Erik M Rauch and Mark M Millonas. The role of trans-membrane signal transduction in turing-type cellular pattern formation. *Journal of Theoretical Biology*, 226(4):401–407, February 2004. URL: `https://www.sciencedirect.com/science/article/pii/S0022519303003588`, `doi:10.1016/j.jtbi.2003.09.018`.

[35] J. Ritchie. Turing instability and pattern formation on directed networks. *Communications in nonlinear science & numerical simulation*, 116:106892–, 2023. Publisher: Elsevier B.V. `doi:10.1016/j.cnsns.2022.106892`.

[36] L. Shen and R. Van Gorder. Predator-prey-subsidy population dynamics on stepping-stone domains. *Journal of Theoretical Biology*, 420, 2017. Publisher: Elsevier. URL: `https://ora.ox.ac.uk/objects/uuid:2e725170-8427-43b4-a589-7400ac7868fa`.

[37] Mingrui Song, Shupeng Gao, Chen Liu, Yue Bai, Lei Zhang, Beilong Xie, and Lili Chang. Cross-diffusion induced Turing patterns on multiplex networks of a predator–prey model. *Chaos, solitons and fractals*, 168:113131–, 2023. Publisher: Elsevier Ltd. `doi:10.1016/j.chaos.2023.113131`.

[38] Taro Takaguchi and Renaud Lambiotte. Sufficient conditions of endemic threshold on metapopulation networks. *Journal of Theoretical Biology*, 380:134–143, September 2015. arXiv:1410.5116 [cond-mat, physics:physics, q-bio]. URL: `http://arxiv.org/abs/1410.5116`, `doi:10.1016/j.jtbi.2015.05.024`.

[39] A. M. Turing. The chemical basis of morphogenesis. *Bulletin of Mathematical Biology*, 52(1):153–197, January 1990. `doi:10.1007/BF02459572`.

[40] Robert A. Van Gorder. A theory of pattern formation for reaction–diffusion systems on temporal networks. *Proceedings of the Royal Society A: Mathematical, Physical and Engineering Sciences*, 477(2247):rspa.2020.0753, 20200753, March 2021. URL: `https://royalsocietypublishing.org/doi/10.1098/rspa.2020.0753`, `doi:10.1098/rspa.2020.0753`.

[41] Vladimir K. Vanag and Irving R. Epstein. Segmented spiral waves in a reaction-diffusion system. *Proceedings of the National Academy of Sciences*, 100(25):14635–14638, December 2003. Publisher: Proceedings of the National Academy of Sciences. URL: `https://www.pnas.org/doi/full/10.1073/pnas.2534816100`, `doi:10.1073/pnas.2534816100`.

[42] Weiming Wang, Xiaoyan Gao, Yongli Cai, Hongbo Shi, and Shengmao Fu. Turing patterns in a diffusive epidemic model with saturated infection force. *Journal of the Franklin Institute*, 355(15):7226–7245, October 2018. URL: `https://www.sciencedirect.com/science/article/pii/S0016003218304915`, `doi:10.1016/j.jfranklin.2018.07.014`.

[43] Qi Xuan, Fang Du, Hui Dong, Li Yu, and Guanrong Chen. Structural control of reaction-diffusion networks. *Physical Review E*, 84(3):036101, September 2011. Publisher: American Physical Society. URL: `https://link.aps.org/doi/10.1103/PhysRevE.84.036101`, `doi:10.1103/PhysRevE.84.036101`.

[44] Nazanin Zaker, Christina A. Cobbold, and Frithjof Lutscher. The effect of landscape fragmentation on Turing-pattern formation. *Mathematical Biosciences and Engineering*, 19(3):2506–2537, January 2022. Number: 3 Publisher: AIMS Press. URL: `https://eprints.gla.ac.uk/261281/`, `doi:10.3934/mbe.2022116`.

[45] Hao Zhang, Yin Sheng, and Zhigang Zeng. Synchronization of Coupled Reaction–Diffusion Neural Networks With Directed Topology via an Adaptive Approach. *IEEE Transactions on Neural Networks and Learning Systems*, 29(5):1550–1561, May 2018. URL: `https://ieeexplore.ieee.org/document/7879312/`, `doi: 10.1109/TNNLS.2017.2672781`.

[46] M. Mocarlo Zheng, Bin Shao, and Qi Ouyang. Identifying network topologies that can generate turing pattern. *Journal of Theoretical Biology*, 408:88–96, November 2016. URL: `https://www.sciencedirect.com/science/article/pii/S0022519316302405`, `doi:10.1016/j.jtbi.2016.08.005`.

[47] Qianqian Zheng and Jianwei Shen. Pattern formation in the FitzHugh–Nagumo model. *Computers & Mathematics with Applications*, 70(5):1082–1097, September 2015. URL: `https://www.sciencedirect.com/science/article/pii/S089812211500317X`, `doi:10.1016/j.camwa.2015.06.031`.

[48] Shijie Zhou, Yao Guo, Maoxing Liu, Ying-Cheng Lai, and Wei Lin. Random temporal connections promote network synchronization. *Physical review. E*, 100(3):032302–032302, 2019. Publisher: American Physical Society. `doi: 10.1103/PhysRevE.100.032302`.